Redox Biology 21 (2019) 101063

Contents lists available at ScienceDirect

Redox Biology

journal homepage: www.elsevier.com/locate/redox

NOXA1-dependent NADPH oxidase regulates redox signaling and phenotype of vascular smooth muscle cell during atherogenesis

Aleksandr E. Vendrov, Arihiro Sumida, Chandrika Canugovi, Andrey Lozhkin, Takayuki Hayami, Nageswara R. Madamanchi[1], Marschall S. Runge[*,1]

Frankel Cardiovascular Center, Department of Internal Medicine, University of Michigan, Ann Arbor, MI 48109, USA

ARTICLE INFO

Keywords:
Oxidative stress
NOXA1
Smooth muscle cells
KLF4
Macrophage-like cells
Atherosclerosis

ABSTRACT

Increased reactive oxygen species (ROS) production and inflammation are key factors in the pathogenesis of atherosclerosis. We previously reported that NOX activator 1 (NOXA1) is the critical functional homolog of p67phox for NADPH oxidase activation in mouse vascular smooth muscle cells (VSMC). Here we investigated the effects of systemic and SMC-specific deletion of *Noxa1* on VSMC phenotype during atherogenesis in mice.

Neointimal hyperplasia following endovascular injury was lower in *Noxa1*-deficient mice versus the wild-type following endovascular injury. *Noxa1* deletion in *Apoe*$^{-/-}$ or *Ldlr*$^{-/-}$ mice fed a Western diet showed 50% reduction in vascular ROS and 30% reduction in aortic atherosclerotic lesion area and aortic sinus lesion volume ($P < 0.01$). SMC-specific deletion of *Noxa1* in *Apoe*$^{-/-}$ mice (*Noxa1*$^{SMC-/-}$/*Apoe*$^{-/-}$) similarly decreased vascular ROS levels and atherosclerotic lesion size. TNFα-induced ROS generation, proliferation and migration were significantly attenuated in *Noxa1*-deficient versus wild-type VSMC. Immunofluorescence analysis of atherosclerotic lesions showed a significant decrease in cells positive for CD68 and myosin11 (22% versus 9%) and Mac3 and α-actin (17% versus 5%) in the *Noxa1*$^{SMC-/-}$/*Apoe*$^{-/-}$ versus *Apoe*$^{-/-}$ mice. The expression of transcription factor KLF4, a modulator of VSMC phenotype, and its downstream targets – VCAM1, CCL2, and MMP2 – were significantly reduced in the lesions of *Noxa1*$^{SMC-/-}$/*Apoe*$^{-/-}$ versus *Apoe*$^{-/-}$ mice as well as in oxidized phospholipids treated *Noxa1*$^{SMC-/-}$ versus wild-type VSMC.

Our data support an important role for NOXA1-dependent NADPH oxidase activity in VSMC plasticity during restenosis and atherosclerosis, augmenting VSMC proliferation and migration and KLF4-mediated transition to macrophage-like cells, plaque inflammation, and expansion.

1. Introduction

Chronic unresolved inflammation in the vascular wall is the pathophysiological basis for progressive atherogenesis and its complications [1]. Increased cellular and mitochondrial oxidative stress is integral to vascular inflammation and atherosclerosis burden in mouse and human arteries [2,3]. NADPH oxidases (NOX) are expressed in vascular wall and inflammatory cells alike and are one of the major sources of reactive oxygen species (ROS) in vasculature [3,4]. Multiple reports provide evidence of association between hyperactivation of NADPH oxidases and vascular diseases, including atherosclerosis and restenosis [5]; however, the molecular composition, tissue distribution and the precise role in the disease process of individual NADPH oxidases remain incompletely understood.

The NADPH oxidase catalytic subunits - NOX1, NOX2, and NOX4 - share a conserved structure and associate with p22phox on the cell membranes and are expressed in the vascular wall cells in rodents and humans [4]. Activation of NOX1/2 NADPH oxidase requires association with activated cytosolic subunits, whereas NOX4 is constitutively active and is regulated at transcriptional level [6]. NOXs complexity is reflected in its diverse tissue and cellular distribution. Expression of NOX4 is ubiquitous in vascular cells, while NOX2 is primarily expressed in endothelial cells, adventitial fibroblasts, and bone marrow derived cells. In contrast, NOX1 is predominantly expressed in vascular smooth

Abbreviations: APOE, apolipoprotein E; CCL2, CC chemokine ligand 2; KLF4, Krüppel-like factor 4; MMP2, matrix metalloproteinase 2; NOX, NADPH oxidase; NOXA1, Nox activator 1; POVPC, 1-palmitoyl-2-(5-oxovaleroyl)-*sn*-glycero-3-phosphatidylcholine; ROS, reactive oxygen species; VCAM1, vascular cell adhesion molecule 1; VSMC, vascular smooth muscle cells

* Correspondence to: Department of Internal Medicine, University of Michigan, 7324 Medical Sciences Building I, 1301 Catherine St., Ann Arbor, MI 48109, USA.
E-mail address: mrunge@med.umich.edu (M.S. Runge).

[1] Both authors are joint senior authors.

https://doi.org/10.1016/j.redox.2018.11.021
Received 19 October 2018; Received in revised form 16 November 2018; Accepted 29 November 2018
Available online 29 November 2018

muscle cells (VSMC) and is one of the primary regulators of VSMC activation [7]. NOX1 expression was also reported in colon epithelial cells and lymphoid tissue [8] and microglia [9] and is critical for macrophage function [10] and differentiation [11].

NOX1 plays a critical role in VSMC function in response to pathophysiological stimuli. The *Nox1* expression is induced in neointimal SMC after vascular injury [12,13] where it mediates cell migration, proliferation, and extracellular matrix production; while *Nox1* deletion significantly reduces neointima hyperplasia [7]. Our previous studies showed that increased ROS levels and expression of inflammatory markers in early stages of atherosclerotic lesion development in *Apoe*$^{-/-}$ mice are mostly mediated by activation of NOX1 NADPH oxidase [14,15]. Consistent with this, NOX1/NOX4 pharmacological inhibitor significantly reduced atherosclerosis burden in young *Apoe*$^{-/-}$ mice fed a Western diet [16]. Moreover, Sheehan et al. demonstrated that deficiency of *Nox1* in *Apoe*$^{-/-}$ mice significantly attenuated vascular ROS levels and atherosclerotic lesion area [17]. It was also suggested that NOX1 is a major source of ROS in vasculature in diabetes as its deletion and pharmacological inhibition in diabetic *Apoe*$^{-/-}$ mice attenuated atherogenesis [18].

We and others previously demonstrated that in mouse VSMC NOXA1 interacts with p47phox and is critical component of NOX1 NADPH oxidase [19,20]. In addition, we showed that localized *Noxa1* overexpression increased ROS production and enhanced neointimal hyperplasia after vascular injury [20]. Expression of NOXA1 was increased in aortas of *Apoe*$^{-/-}$ mice and in early stages of atherosclerosis in human carotid arteries.

Vascular SMC play major role in atherogenesis and atherosclerotic plaque evolution by sustaining vascular wall ROS generation and inflammation and matrix remodeling [21]. Furthermore, our studies demonstrated that these processes are enhanced during aging- and ROS-driven expansion and remodeling of atherosclerotic plaque, increasing necrotic core and thinning fibrous cap [22,23]. Recent data suggest that VSMC in the atherosclerotic lesions undergo phenotypic transition to macrophage-like cells that express both macrophage and SMC markers and promote inflammation and enhanced atherogenesis [24]. In addition, activation of transcription factor Krüppel-like factor 4 (KLF4) by oxidized phospholipids promoted VSMC phenotypic modulation in mouse and human atherosclerotic lesions [25].

In the present study we tested the effects of NOXA1 deficiency on the function and phenotypic fate of SMC in vascular remodeling and atherogenesis using newly characterized *Noxa1*$^{-/-}$ mice and SMC-specific *Noxa1* knockouts. *Noxa1*-deficient mice had attenuated neointima proliferation and vessel wall remodeling in response to endovascular injury as well as lower arterial wall ROS levels and atherosclerotic lesion size in hypercholesterolemic mice. *Noxa1* deletion attenuated ROS levels and MAP kinases activity, migration and proliferation of cultured VSMC and reduced SMC phenotypic modulation in atherosclerotic lesions resulting in decreased intraplaque inflammation and matrix remodeling.

2. Materials and methods

2.1. Animals

All animal procedures were performed in compliance with the protocols approved by University of Michigan Institutional Animal Care and Use Committee in accordance with NIH OLAW policy. Male wild-type C57BL/6J, *Apoe*$^{-/-}$ (B6.129P2-*Apoe*^{tm1Unc}/J) and *Ldlr*$^{-/-}$ (B6.129S7-*Ldlr*^{tm1Her}/J) mice were purchased from The Jackson Laboratory (Bar Harbor, ME). The *Noxa1*$^{-/-}$ mice were generated by inGenious Targeting Laboratory (iTL, Stony Brook, NY) by removing the coding region of mouse *Noxa1* gene. IC1 (C57BL/6) embryonic stem cells were transfected by electroporation with *Not*I-linearazed targeting vector containing LoxP/FRT-Neomycin (Neo) cassette flanked by two homology arms that span the entire 12 exons of *Noxa1* gene. After selection with G418 antibiotic, recombinant clones were identified by PCR and Southern blot analysis. Targeted IC1 embryonic stem cells (C57BL/6) were microinjected into BALB/c-derived blastocysts and implanted into uterus of pseudopregnant females. Resulting chimeras with high percentage black coat color were mated with wild-type C57BL/6 mice to generate F1 heterozygous offspring. Tail DNA from F1 pups with black coat color was analyzed by PCR for presence of Neo cassette and by Southern blot to confirm germline-transmitted *Noxa1* deletion. Positively identified mice were bred with ACTB: FLPe B6J (B6. Cg-Tg (ACTFLPe)9205Dym/J) mice to delete Neo cassette and any additional tandem integrations. Resulting F2 mice were screened for Neo cassette deletion and bred with wild-type C57BL/6 mice. The pups were screened by PCR to identify germline Neo-deleted mice and for absence of FLP transgene. The knock-out of *Noxa1* gene was confirmed by Southern blot analysis and PCR genotyping. Primers used for genotyping were NDEL1: GCTTCCTGGCAAGAACTAGGAG; NDEL2: GACCA GACAGTCAGAGTCCAGCT; WT1: AGGGTAAAGGGCAGGGATTC. *Noxa1*-deficient heterozygote mice were backcrossed with C57BL/6 wild-type mice for ten generations before the colony was used in experiments. The *Noxa1*$^{-/-}$ mice were crossed with *Apoe*$^{-/-}$ to generate *Noxa1*$^{-/-}$/*Apoe*$^{-/-}$ mice and with *Ldlr*$^{-/-}$ to generate *Noxa1*$^{-/-}$/*Ldlr*$^{-/-}$ mice.

Mice carrying *Noxa1* conditional allele (B6(Cg)-*Noxa1*^{tm1Brg}/BrgJ) [26] and SM22α-CreKI mice (B6.129S6-*Tagln*$^{tm2(cre)Yec}$/J) were acquired from The Jackson Laboratory and crossed in-house to generate smooth muscle-specific *Noxa1*-null homozygotes *Noxa1*$^{flox/flox}$/SM22α-CreKI (*Noxa1*$^{SMC-/-}$). SM22α-CreKI mice were crossed with ROSA26-GNZ-KI (B6.129-*Gt(ROSA)26Sor*^{tm1Joe}/J) to assess SMC-specific Cre activity. The *Noxa1*$^{flox/flox}$, SM22α-CreKI, and *Noxa1*$^{flox/flox}$/SM22α-CreKI mice were crossed with *Apoe*$^{-/-}$ to generate *Noxa1*$^{flox/flox}$/*Apoe*$^{-/-}$, SM22α-CreKI/ *Apoe*$^{-/-}$, and *Noxa1*$^{flox/flox}$/SM22α-CreKI/*Apoe*$^{-/-}$ (*Noxa1*$^{SMC-/-}$/*Apoe*$^{-/-}$) mice.

Littermate male mice from heterozygous breeding were used in all experiments. All mice were housed in ventilated cages at 22 °C with a 12 h light/dark cycle with free access to food and water. For atherosclerosis analysis, mice (n = 12) were fed standard rodent chow until 8 weeks of age and then Western diet (TD.88137; Envigo, Madison, WI) for 12 weeks. The femoral artery endovascular injury was performed in 10-week old wild-type and *Noxa1*$^{-/-}$ mice (n = 7) as previously described [20]. Briefly, mice were anesthetized with inhaled 2% isoflurane (MWI, Boise, ID), the right femoral artery was dissected from adjacent tissues, and Hi-Torque Floppy II angioplasty guide wire (0.014" tip; Abbott Laboratories, Chicago, IL) was introduced through arteriotomy and passed five times to denude the endothelium. The guide wire was removed and arteriotomy site ligated with 9–0 nylon suture. The skin incision was closed with 6–0 silk suture. The left femoral artery was sham-operated without introduction of the guide wire. Animals were sacrificed 21 days after injury.

2.2. Cell culture and siRNA transfection

VSMC were isolated from aortas of wild-type, *Noxa1*$^{-/-}$, SM22α-CreKI, and *Noxa1*$^{flox/flox}$/SM22α-CreKI (*Noxa1*$^{SMC-/-}$) mice as described previously [27]. Cells were cultured in Dulbecco's modified Eagle's medium (DMEM) supplemented with 10% fetal bovine serum (FBS) and antibiotic/antimycotic solution (Thermo Fisher Scientific, Waltham, MA) in a 5% CO_2 incubator at 37 °C. Experiments were performed using cells between passages 3 and 10. Cells were growth arrested for 24 h in FBS-free DMEM and then treated with 100 ng/ml TNFα (R&D Systems, Minneapolis, MN), 10 μg/ml 1-palmitoyl-2-(5-oxovaleroyl)-*sn*-glycero-3-phosphatidylcholine (POVPC; Cayman Chemical, Ann Arbor, MI) or 20 μM diphenyliodonium (DPI; Sigma-Aldrich, St. Louis, MO).

Mouse *Map4k4* ON-TARGETplus SMARTpool siRNA (L-040100–00) and nontargeting siRNA control (D-001810-01) were purchased from Dharmacon (Lafayette, CO). VSMC were transfected with siRNAs using Lipofectamine RNAiMAX Transfection Reagent (Thermo Fisher) as described previously [23].

2.3. ROS detection

In cultured VSMC treated with TNFα or DPI the ROS levels were determined immediately after sample collection. Cellular ROS levels were assessed by measuring CM-H_2DCFDA (Thermo Fisher) fluorescence as described [20]. Superoxide generation levels were determined by HPLC analysis of 2-hydroxyethidium (Thermo Fisher) as described previously [27]. Hydrogen peroxide generation was measured with Amplex Red assay as described previously [27]. All measurements were performed with appropriate controls to correct for background signal using PEG-SOD or PEG-catalase (Sigma-Aldrich). All values were normalized to VSMC protein concentration.

Tissue samples for ROS detection in situ were snap frozen in liquid nitrogen and frozen sections were analyzed immediately after collection. ROS levels in aortic root sections were detected with DHE fluorescence as described [27]. Fluorescence images were taken using a Nikon Microphot-FX microscope with 510 nm excitation/580 nm emission filters. Grayscale images were analyzed with NIH ImageJ 1.51 software (Bethesda, MD) to determine integrated density. Controls incubated with PEG-SOD were used to correct for background fluorescence.

2.4. Histology, immunostaining, and Western Blot analysis

Mice were euthanized with inhaled isoflurane overdose, the circulatory system was cleared by transcardial perfusion with 20 ml phosphate-buffered saline (PBS), aortas were dissected and fixed in 3.7% formaldehyde (Thermo Fisher), opened longitudinally, pinned on black wax, stained with 1% oil red O, and counterstained with 0.1% toluidine blue (Sigma-Aldrich). Digital images of stained aortas were analyzed with NIH ImageJ in a blinded manner. Mouse aortic roots were embedded in O.C.T. compound (Sakura Finetek, Torrance, CA), snap-frozen in liquid nitrogen and transverse serial sections were cut at 5 μm thickness starting at the level of aortic valve with 50 μm interval between series and then stained with oil red O/hematoxylin (Sigma-Aldrich). Aortic root lesion volume was calculated by integration of serial sections atherosclerotic lesion area. Immunofluorescence analysis was performed as described [23]. Aortic root sections were fixed in acetone, blocked with normal goat serum and consecutive sections were stained using AlexaFluor 594-conjugated CD68, AlexaFluor 488-conjugated smooth muscle MHC (Bioss, Woburn, MA), FITC-conjugated Mac3 (M3/84) (Thermo Fisher Scientific), Cy3-conjugated α-smooth muscle actin (Sigma-Aldrich), and KLF4 (Abcam), VCAM1, CCL2, MMP2 (Bioss) and MAP4K4 (Cell Signaling Technology, Danvers, MA) followed with AlexaFluor 594-conjugated goat anti-rabbit antibody and FITC-conjugated α-smooth muscle actin (Sigma-Aldrich). Sections were mounted with Vectashield mounting medium with DAPI (Vector Laboratories, Burlingame, CA).

Mice that underwent femoral artery injury were euthanized with inhaled isoflurane overdose; the circulatory system was cleared by transcardial perfusion with 20 ml PBS followed by 20 ml of 3.7% formaldehyde. The femoral arteries with surrounding muscle tissue were dissected and fixed in 3.7% formaldehyde for 24 h. Tissues were paraffin embedded and 5 μm serial sections were collected every 250 μm distal to the ligature through the length of the tissue block. Serial sections were stained with Masson's trichrome stain and morphometric analysis performed in a blinded manner using NIH ImageJ 1.51. For immunofluorescence, sections were deparaffinized, rehydrated and antigen retrieval was performed using Retrievagen A (BD Biosciences, San Jose, CA). Consecutive sections were stained using antibodies against NOX1 (Abcam), NOXA1 (Ab199, gift of Prof. Dr. Ralf P. Brandes, Goethe University, Frankfurt am Main, Germany) [20], and p67phox (Bioss) following with AlexaFluor 594-conjugated goat anti-rabbit antibody. Sections were costained with FITC-conjugated anti-α-smooth muscle actin antibody and mounted with Vectashield mounting medium with DAPI (Vector Laboratories). Images were acquired with Nikon Microphot-FX microscope and analyzed using NIH ImageJ 1.51.

Frozen transverse aortic sections from *Noxa1*$^{SMC-/-}$ and wild-type mice were stained using NOXA1antibody (EMD Millipore) and VECTASTAIN Elite ABC kit and Vector DAB substrate kit (Vector Laboratories). Frozen transverse aortic sections from ROSA26-GNZ KI/SM22α-CreKI mice were stained using β-galactosidase Reporter Gene Staining kit following manufacturer's recommendations (Sigma-Aldrich).

Western blot analysis was performed as described previously [27]. The primary antibodies used were against phosphorylated and total ERK1/2, p38 MAPK, JNK, AKT, JAK2, STAT3, MAP4K4 (Cell Signaling), and KLF4 (Abcam), CD68 (Bioss), α-smooth muscle actin (1A4), and β-tubulin (Santa Cruz Biotechnology, Dallas, TX).

2.5. Flow cytometry analysis

Mice were euthanized with inhaled isoflurane overdose and the circulatory system was cleared by perfusion with PBS. Aortas were dissected and incubated with collagenase type II (175 U/ml) to remove adventitia. Aortas were minced and placed into an enzyme cocktail (collagenase type I 450 U/ml, collagenase type XI 125 U/ml, hyaluronidase 60 U/ml). Cell suspension was passed through a 70 μM cell strainer (Corning, Corning, NY) and washed with FACS buffer (PBS, 1% BSA, 1 mM EDTA). Samples were fixed and permeabilized with Foxp3/Transcription Factor Staining Buffer Set (Thermo Fisher). Cells were blocked with rat anti-mouse CD16/CD32 antibody (BD Biosciences) and stained with PE-conjugated anti-CD68 (BioLegend, San Diego, CA) and FITC-conjugated anti-α-smooth muscle actin (Sigma-Aldrich) antibodies for 45 min 4 °C. The samples were run on MoFlo Astrios EQ (Beckman Coulter, Indianapolis, IN) and data were analyzed with FlowJo v10 (FlowJo, LLC, Stanford University, CA).

2.6. Real-time PCR analysis

Total RNA was extracted from VSMC treated with POVPC (1-palmitoyl-2-(5-oxovaleroyl)-*sn*-glycero-3-phosphocholine) or TNFα using RNeasy Micro Kit (Qiagen, Germantown, MD) and cDNA synthesis was performed using iScript Reverse Transcription Supermix (Biorad, Hercules, CA). Real-time reverse transcription PCR was done as described [23], using TaqMan Gene Expression Assays for *Klf4* (Mm00516104_m1), *Vcam1* (Mm01320970_m1), *Ccl2* (Mm00441242_m1), *Ccl5* (Mm013024228_m1), *Il6* (04446190_m1), *Mmp2* (Mm00439508_m1), and *18s* (Hs99999901_s1) (Thermo Fisher).

2.7. [^{3}H]-thymidine incorporation assay

VSMC from wild-type and *Noxa1*$^{-/-}$ mice were treated with 100 ng/ml TNFα for 20 h and [^{3}H]-thymidine was added for the next 4 h. Assessment of DNA synthesis was performed by liquid scintillation counting as described before [14,20].

2.8. In vitro migration assay

Migration of wild-type and *Noxa1*$^{-/-}$ VSMC after TNFα treatment was determined in a scratch wound assay by measuring maximal wound healing distance as previously described [20].

2.9. Plasma biochemical analysis

Plasma samples were collected from fasted mice through cardiac puncture as described [27]. Plasma cholesterol and triglycerides levels were measured using the AMS Lyasis 330 Clinical Chemistry System (AMS Diagnostics, Weston, FL).

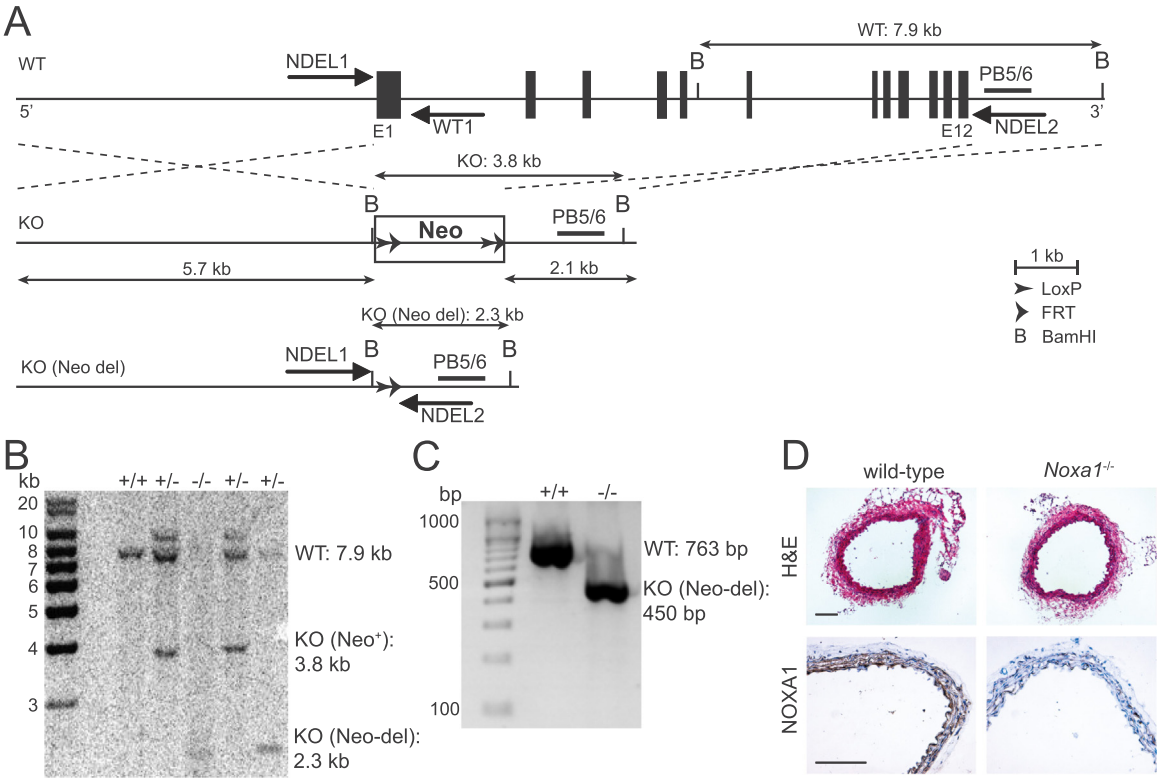

Fig. 1. Generation of *Noxa1*$^{-/-}$ mice. A, Schematic representation of targeting vector containing LoxP/FRT-Neo cassette used for *Noxa1* gene deletion. Location of Southern blot probe (PB5/6) and genotyping primers (WT1, NDEL1, and NDEL2) is shown in relation to wild-type (WT), knock-out Neo present (KO Neo^{+}), and knock-out Neo-deleted (KO Neo-del) of *Noxa1* gene exon structure (E1-E12). **B**, Southern blot analysis of genomic DNA fragments generated after BamHI digestion from *Noxa1* wild-type (+/+), heterozygous (+/-), and knock-out (-/-) mice using PB5/6 probe. **C**, PCR analysis of genomic DNA extracted using genotyping primers WT1, NDEL1, and NDEL2. **D**, Representative images transverse aortic sections from wild-type and *Noxa1*$^{-/-}$ mice stained with H&E (top panel) or immunohistochemistry using NOXA1 antibody (bottom panel). Scale is 100 μm.

Table 1
Body weight (g) and plasma lipids levels (mg/dL) in wild-type, *Apoe*$^{-/-}$, and *Ldlr*$^{-/-}$ mice with *Noxa1* deletion after 12 weeks of Western diet. Data are mean ± SEM, n = 9–12.

	Wild-type	*Noxa1*$^{-/-}$	*Apoe*$^{-/-}$	*Noxa1*$^{-/-}$/*Apoe*$^{-/-}$	*Ldlr*$^{-/-}$	*Noxa1*$^{-/-}$/*Ldlr*$^{-/-}$
Body weight	43.1 ± 1.0	41.3 ± 1.5	31.2 ± 1.1	33.2 ± 1.0	29.0 ± 0.5	30.1 ± 1.3
Cholesterol	210.8 ± 27.2	196.1 ± 16.0	815.8 ± 37.2	831.3 ± 38.9	839.8 ± 35	879.7 ± 70
Triglycerides	94.75 ± 7.7	114.4 ± 8.8	159.6 ± 23.2	156.8 ± 12.5	231.1 ± 17.5	208.5 ± 23.8

2.10. Statistical analysis

All analyses were performed using JMP Pro 13.1.0 (SAS Institute, Cary, NC) or Prism 7 (GraphPad Software, La Jolla, CA). Data sets were tested for normality with Shapiro-Wilk test. All data were analyzed by unpaired *t*-test or one-way ANOVA followed by Tukey's multiple comparisons test. Differences were considered significant at $P < 0.05$.

3. Results

3.1. Generation and characterization of Noxa1-deficient mice

To achieve *Noxa1* gene deletion, the vector containing LoxP/FRT-Neo cassette was designed that targeted genomic region spanning the entire 12 exons in the same direction as the *Noxa1* gene (Fig. 1A). Microinjection of targeted IC1 embryonic stem cells (C57BL/6) yielded mosaic chimeras that were mated with wild-type C57BL/6 to generate F1 heterozygotes. To delete Neo cassette, as well as possible additional tandem integrations, F1 mice were crossed with C57BL/6 FLP transgenic mice. Southern blot analysis of BamHI-digested genomic DNA with PB5/6 probe showed predicted bands with size of 7.9 kb in wild-type, 3.8 kb in Neo^{+} knockout, and 2.3 kb in Neo-deleted knockout mice (Fig. 1B). Resulting *Noxa1*-deficient heterozygote mice were backcrossed to C57BL/6 wild-type mice and knockouts were identified by PCR genotyping (Fig. 1C). *Noxa1*-deficient mice grew normally and did not show any gross abnormalities. Histological analysis of transverse aortic sections from wild-type and *Noxa1*$^{-/-}$ mice showed similar morphology and media thickness. Immunohistochemical staining demonstrated robust expression of NOXA1 in aorta medial layer of wild-type but not *Noxa1*$^{-/-}$ mouse (Fig. 1D). *Noxa1*$^{-/-}$ mice were similar to the wild-type in body weight and plasma cholesterol and triglycerides levels after 12 weeks of Western diet (Table 1).

3.2. Noxa1deficiency attenuates neointima hyperplasia after endovascular wire injury

Inflammation, increased cytokine levels and VSMC proliferation are integral to arterial wound repair; however, its dysregulation causes excessive neointima formation, which is associated with cardiovascular events [28]. We previously showed that enhanced ROS generation from localized overexpression of NOXA1 in arterial SMC results in injured carotid arteries induced neoinitimal thickening [20]. To determine

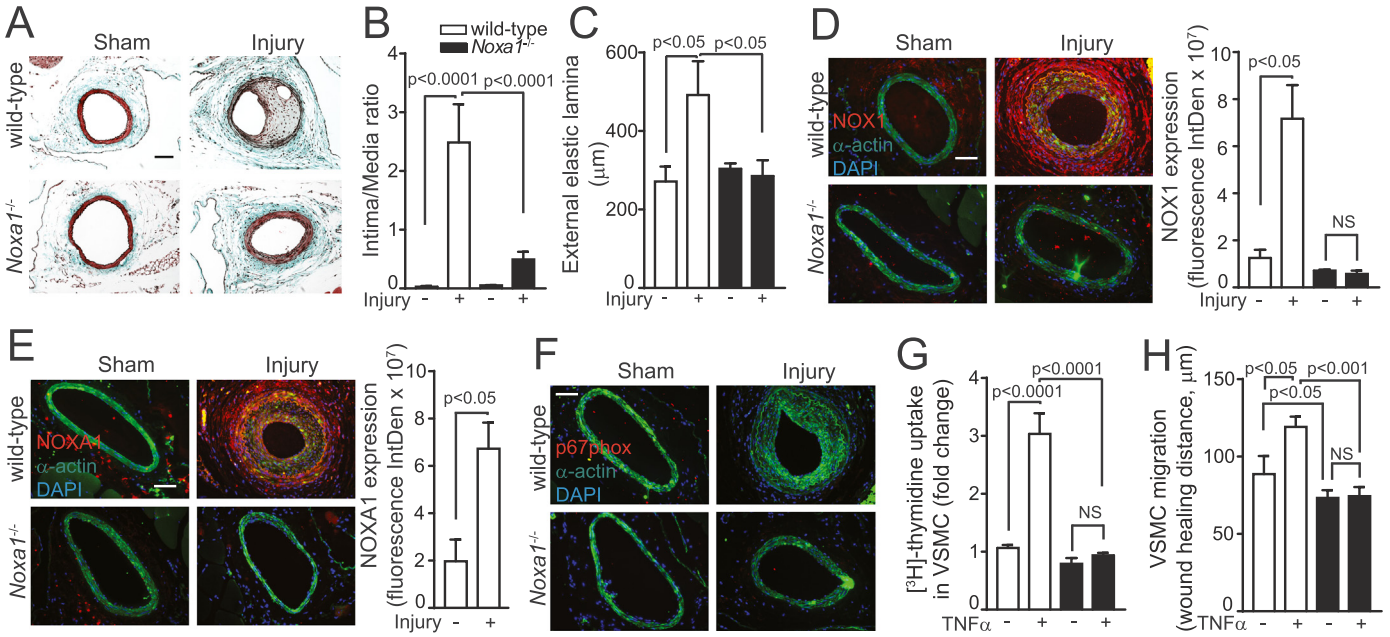

Fig. 2. Neointima hyperplasia after arterial injury is reduced in *Noxa1*$^{-/-}$ compared with wild-type mice and correlates with reduced VSMC proliferation and migration. A, Representative images of femoral artery cross sections stained with Masson's trichrome. B, Quantification of intima/media ratio. C, External elastic lamina circumference (B and C, mean ± SEM, n = 7). D-F, Representative immunofluorescence images and quantification of immunoreactive NOX1 (D), NOXA1 (E), and p67phox (F) – red, and costained with smooth muscle α-actin (green) and DAPI (blue). Data presented are mean ± SEM, n = 5. Scale is 100 μm. G, Quiesced VSMC were treated with 100 ng/ml for 24 h and [^{3}H]-thymidine incorporation was measured during the last 4 h. Data, normalized to protein concentration, are mean ± SEM (n = 4). H, VSMC migration was assessed by scratch wound assay with and without 100 ng/ml of TNFα stimulation for 24 h and maximal wound healing distance is presented as mean ± SEM (n = 4).

whether endogenous NOXA1-dependent NADPH oxidase activity is critical in arterial neointimal hyperplasia, we examined femoral arteries after guide wire injury in wild-type and *Noxa1*$^{-/-}$ mice. Femoral arteries cross sections post-injury demonstrated markedly enhanced neoinitimal hyperplasia in the wild-type mice in contrast with minimal or complete absence of neointima in *Noxa1*$^{-/-}$ mice (Fig. 2A). Morphometric analysis of femoral arteries showed higher neointima/media ratio ($P < 0.0001$ versus *Noxa1*$^{-/-}$; Fig. 2B) and outward remodeling in the wild-type versus sham operated wild-type (80% increase) and *Noxa1*$^{-/-}$ mice ($P < 0.05$; Fig. 2C). Another mechanism for NOXA1-dependent NADPH oxidase activation is via increased expression of NOX1 in injured arteries [12]. Consistent with this notion, immunoreactive NOX1 expression increased markedly in medial and neointimal VSMC of injured arteries of the wild-type mice. In contrast, NOX1 expression was minimal in femoral arteries of *Noxa1*$^{-/-}$ mice and wire injury had no effect on NOX1 expression levels (Fig. 2D), suggesting that NOXA1-dependent NADPH oxidase activity induced by inflammatory mediators from damaged cells might enhance NOX1 expression. In concert with induced NOX1 levels, expression of immunoreactive NOXA1 was also increased in medial and neointimal SMC of injured arteries from the wild-type and was absent in *Noxa1*$^{-/-}$ mice (Fig. 2E). Expression of immunoreactive p67phox was not observed in medial or neointimal SMC in sham-operated or injured arteries of either genotype (Fig. 2F). Taken together, these results confirm the role of NOXA1-dependent NADPH oxidase in arterial SMC hyperplasia and vessel wall remodeling in response to injury.

The proinflammatory cytokine TNFα, secreted by macrophages, endothelium and VSMC, localizes in areas of arterial injury and promotes the development of neointimal hyperplasia by inducing VSMC matrix metalloproteinase expression, migration and proliferation [29]. In addition, we previously showed that TNFα is a potent inducer of NOXA1 expression in mouse VSMC [20]. To determine how NOXA1 regulates neointima formation in response to arterial injury, we examined the role of NOXA1-dependent NADPH oxidase activity in TNFα-induced VSMC proliferation and migration. TNFα significantly increased DNA synthesis in the wild-type but not in *Noxa1*$^{-/-}$ cells (185% versus 20%, respectively; Fig. 2G) as measured by [^{3}H]-thymidine incorporation assay. Similarly, both basal and TNFα-stimulated cell migration, determined by wound healing distance, was significantly higher in the wild-type versus *Noxa1*$^{-/-}$ cells (Fig. 2H). These results further support the notion that NOXA1-dependent NADPH oxidase activation exacerbates the arterial repair response and excessive neointima formation by mediating the effects of cytokines such as TNFα and other agonists released at the site of injury.

3.3. Atherosclerotic lesion size is reduced in Noxa1-deficient Apoe-/- and Ldlr-/- mice

Because NOXA1 expression is increased in atherosclerotic lesions of *Apoe*$^{-/-}$ mice and early atherosclerotic lesions in human carotid arteries [20], we next investigated whether deletion of *Noxa1* decreases atherosclerosis burden in *Apoe*$^{-/-}$ mice. *En face* analysis of aortas from mice fed Western diet for 12 weeks showed a 30% reduction in atherosclerotic lesions size in *Noxa1*$^{-/-}$/*Apoe*$^{-/-}$ compared with *Apoe*$^{-/-}$ mice, with the greatest reduction in thoracic and abdominal aorta ($P = 0.0002$; Fig. 3A). Analysis of serial transverse sections through the aortic sinus also showed a significant decrease in lesion area and integrated lesion volume in *Noxa1*$^{-/-}$/*Apoe*$^{-/-}$ mice (Fig. 3B). The ROS levels, determined by DHE fluorescence in the aortic sinus transverse sections, were significantly lower in the *Noxa1*$^{-/-}$/*Apoe*$^{-/-}$ compared with *Apoe*$^{-/-}$ mice (Fig. 3C). Deletion of *Noxa1* had no significant effect on plasma cholesterol and triglyceride levels or body weight in *Apoe*$^{-/-}$ mice (Table 1).

Since *Apoe* deficiency may induce atherosclerotic lesion development by mechanisms other than its effects on lipid metabolism and the plasma lipoprotein profile of *Ldlr*$^{-/-}$ mice resembles that of humans [30,31], we also tested effects of *Noxa1*-deficiency on atherosclerosis burden in *Noxa1*$^{-/-}$/*Ldlr*$^{-/-}$ mice. In general, atherosclerotic lesion size in aortas of *Ldlr*$^{-/-}$ mice fed a Western diet for 12 weeks was lower compared with *Apoe*$^{-/-}$ mice. Similar to *Apoe*$^{-/-}$ mice, *Noxa1* deletion in

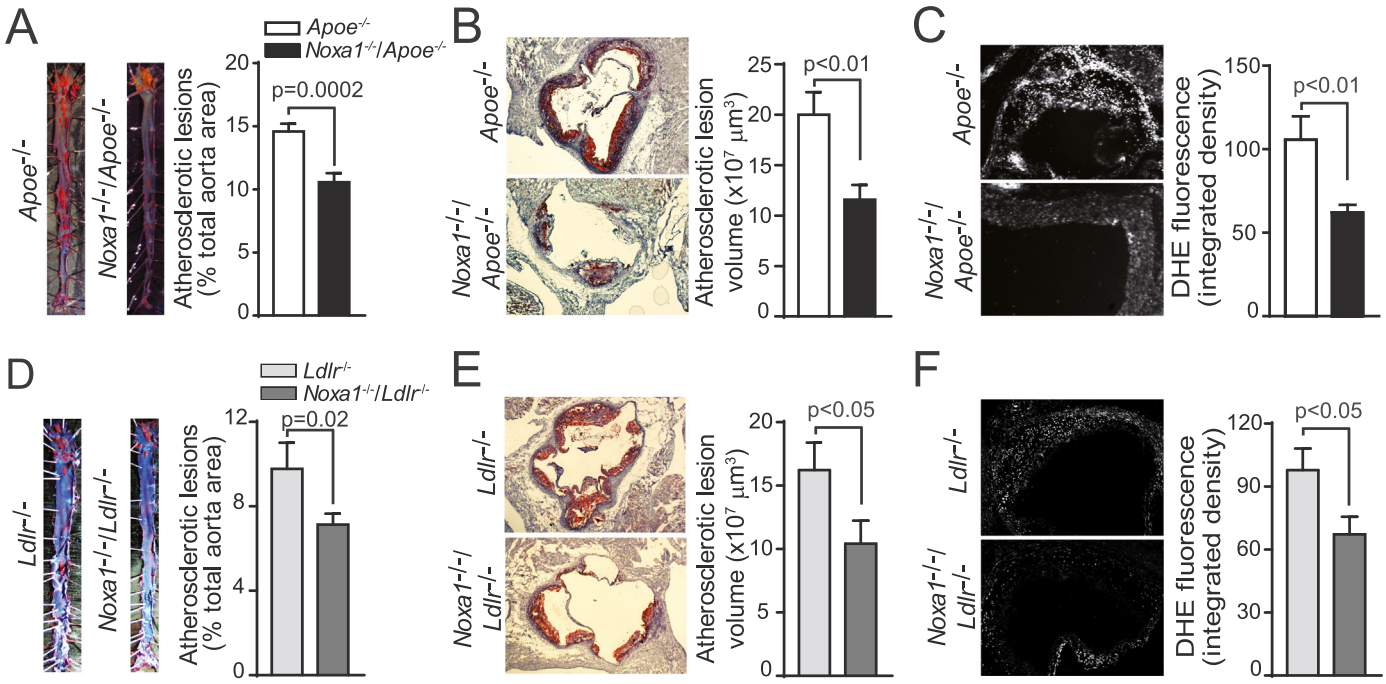

Fig. 3. *Noxa1* deletion attenuates ROS levels and atherogenesis in *Apoe*$^{-/-}$ and *Ldlr*$^{-/-}$ mice fed a Western diet. A, Representative images and quantification of en face oil red O-positive area of aortas (mean ± SEM, n = 12). **B**, Representative images and quantification of lesion volume of oil red O stained aortic root sections. Data presented was atherosclerotic lesion volume integrated from serial transverse sections (mean ± SEM, n = 12). **C**, Representative images and quantification of DHE fluorescence in aortic root sections. Data presented was integrated density of DHE fluorescence (mean ± SEM, n = 8). **D**, Representative images and *en face* analysis of oil red O-positive area of aortas (mean ± SEM, n = 10). **E**, Representative images and quantification of lesion volume of oil red O stained aortic root sections. Atherosclerotic lesion volume was integrated from serial transverse sections (mean ± SEM, n = 9). **F**, Representative images and quantification of DHE fluorescence in aortic root sections (mean ± SEM, n = 9). Scale is 100 µm.

Ldlr$^{-/-}$ mice reduced lesion size by 30% (P = 0.02; Fig. 3D), without a significant effect on plasma lipid levels (Table 1). Aortic sinus lesion area and integrated volume were significantly lower in *Noxa1*$^{-/-}$/*Ldlr*$^{-/-}$ compared with *Ldlr*$^{-/-}$ mice (Fig. 3E). Furthermore, ROS levels in the aortic sinus atherosclerotic lesions were also significantly lower in *Noxa1*$^{-/-}$/*Ldlr*$^{-/-}$ mice (Fig. 3F). Taken together, these results support that NOXA1-containing NADPH oxidase activity significantly increases ROS levels in the aortic wall and is critical in atherogenesis under hyperlipidemic conditions, contributing to increased lesion size and volume.

3.4. Smooth muscle-specific deletion of Noxa1results in decreased atherogenesis in Apoe-/- mice

To confirm the atherogenic effects of NOXA1-dependent NADPH oxidase activation in VSMC, we generated mice with SMC-specific deletion of *Noxa1* allele, *Noxa1*$^{SMC-/-}$ (*Noxa1*$^{flox/flox}$/SM22α-CreKI). Immunoreactive NOXA1 was not detected in aortas of *Noxa1*$^{SMC-/-}$ mice compared with the wild-type mice whereas there was no difference in NOXA1 expression in colon epithelium (Fig. 4A). The SMC-specific Cre activity was also confirmed by positive X-gal staining in aortas of ROSA26-GNZ-KI/SM22α-CreKI mice (Fig. 4B). *Noxa1*$^{SMC-/-}$ mice showed normal growth without any gross abnormalities.

We then determined the function of NOXA1 in VSMC biology during atherogenesis in *Noxa1*$^{SMC-/-}$ mice crossed to *Apoe*$^{-/-}$ mice. Analysis of aortic atherosclerotic lesions in *Noxa1*$^{SMC-/-}$/*Apoe*$^{-/-}$ mice fed a Western diet for 12 weeks showed more than 30% reduction of lesion area compared with control *Apoe*$^{-/-}$ mice (*Noxa1*$^{flox/flox}$/*Apoe*$^{-/-}$ and SM22α-CreKI/*Apoe*$^{-/-}$) (Fig. 4C). Aortic sinus atherosclerotic lesion volume was also significantly reduced in *Noxa1*$^{SMC-/-}$/*Apoe*$^{-/-}$ compared with *Apoe*$^{-/-}$ mice (Fig. 4D). ROS levels in the aortic sinus were 40% lower in *Noxa1*$^{SMC-/-}$/*Apoe*$^{-/-}$ versus *Apoe*$^{-/-}$ mice (Fig. 4E). VSMC-specific deletion of *Noxa1* did not have a significant effect on body weight and lipid metabolism of *Apoe*$^{-/-}$ mice (Table 2). These data affirm the important role of NOXA1-dependent NADPH oxidase activity in atherogenesis under hyperlipidemic conditions and suggest that dysregulation of VSMC function in itself is sufficient to make a critical difference in atherosclerotic burden.

To further determine VSMC function in atherogenesis, we assessed atherosclerotic plaque morphology in *Noxa1*$^{SMC-/-}$/*Apoe*$^{-/-}$ and *Apoe*$^{-/-}$ mice. Transverse aortic sinus sections stained for immunoreactive CD68 and SM α-actin revealed markedly reduced plaque necrotic core area in *Noxa1*$^{SMC-/-}$/*Apoe*$^{-/-}$ mice; however, no changes in fibrous cap thickness and cellular morphology was observed (Fig. 4F). The fraction of SM α-actin^{+} cells in the cap region was not different but was significantly reduced in the core region of atherosclerotic plaques of *Noxa1*$^{SMC-/-}$/*Apoe*$^{-/-}$ versus *Apoe*$^{-/-}$ mice (Fig. 4G). Similarly, Noxa1 deletion significantly decreased fraction of CD68^{+} cells in the plaque core but had no effect in the cap region (Fig. 4H). These results suggest that *Noxa1* deletion in SMC during atherogenesis may positively affect plaque morphology by reducing necrotic core size without adversely changing fibrous cap cellular composition.

3.5. NOXA1regulates TNFα-induced ROS and redox-sensitive protein kinases activation in VSMC

High plasma TNFα levels in patients were associated with atherosclerosis severity as well as unstable plaques [32,33]. Further supporting its role in atherogenesis, deletion of TNFα inhibited fatty-streak lesion formation in *Apoe*$^{-/-}$ mice [34]. We previously demonstrated that impaired agonist-induced ROS generation is atheroprotective by attenuating VSMC proliferation and migration, key events in atherogenesis [20,35]. To elucidate molecular mechanisms underlying the atheroprotection in *Noxa1*$^{SMC-/-}$/*Apoe*$^{-/-}$ mice, we investigated TNFα-induced redox-sensitive protein kinase activation in VSMC from the wild-type and *Noxa1*$^{SMC-/-}$ mice.

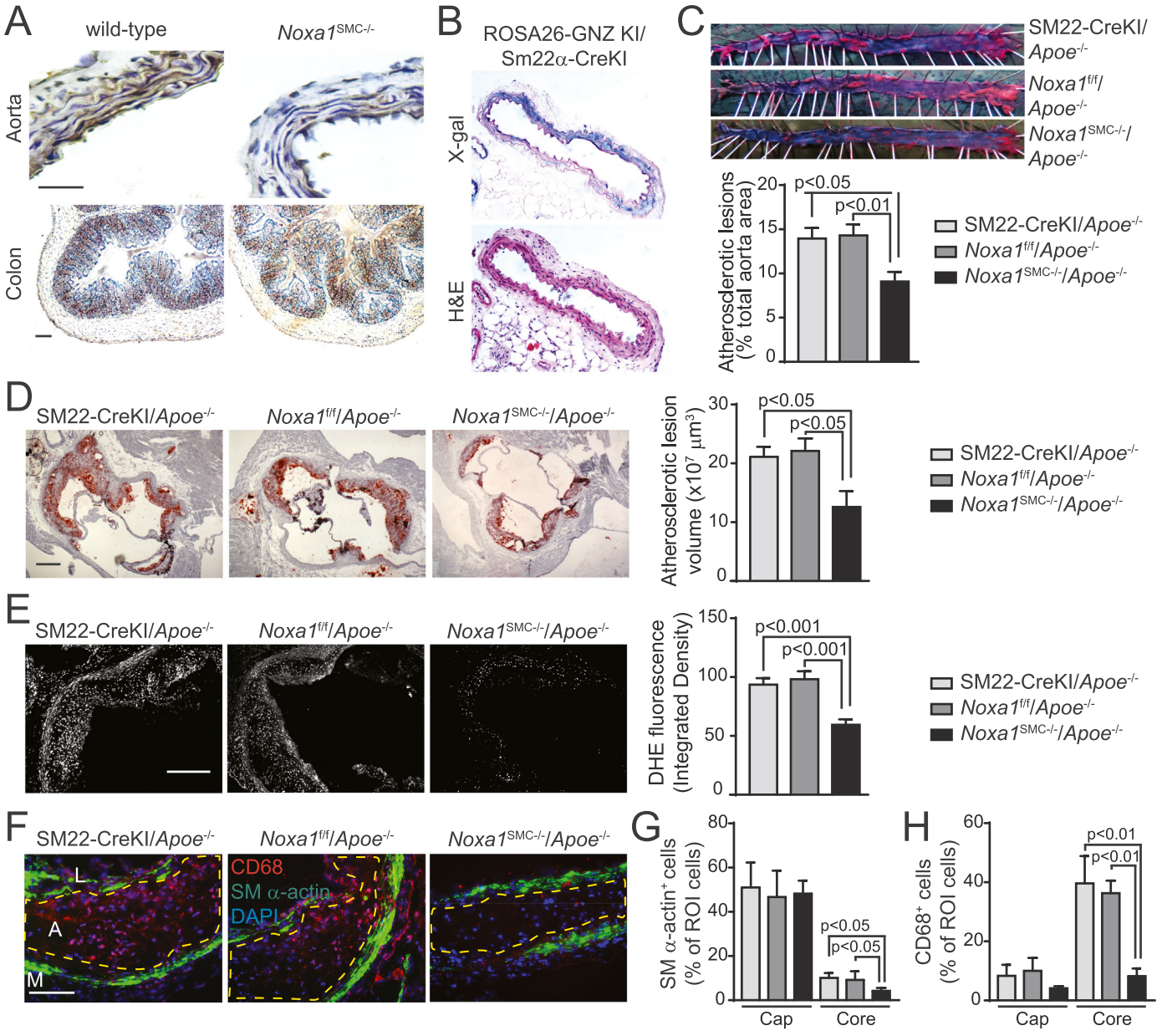

Fig. 4. Smooth muscle-specific deletion of *Noxa1* reduces vascular ROS and atherosclerotic lesion size in *Apoe*$^{-/-}$ mice. A, Representative images of aorta and colon transverse sections immunostained for NOXA1. **B**, Representative sections of aortas from ROSA26-GNZ KI/SM22α-CreKI mice stained with X-gal and hematoxylin & eosin. **C**, Representative images and en face analysis of oil red O-stained aortas from SM22-CreKI/*Apoe*$^{-/-}$, *Noxa1*$^{f/f}$/*Apoe*$^{-/-}$ and *Noxa1*$^{SMC-/-}$/*Apoe*$^{-/-}$ mice (mean ± SEM, n = 10). **D**, Representative images and quantification of lesion volume of oil red O stained aortic sinus sections from *Apoe*$^{-/-}$ and *Noxa1*$^{SMC-/-}$/*Apoe*$^{-/-}$ mice. Atherosclerotic lesion volume was integrated from serial transverse sections (mean ± SEM, n = 10). **E**, Representative images and quantification of DHE fluorescence in aortic root sections (mean ± SEM, n = 10). **F**, Representative images of aortic sinus atherosclerotic lesions stained for immunoreactive CD68 (red), SM-α-actin (green) and with DAPI (blue). Dashed line denotes the plaque necrotic core region. L indicates the lumen; A, atheroma; M, media. **G**, Quantification of SM-α-actin^{+} cells in the cap and core region of atherosclerotic plaque as a percent of cells in the region of interest (ROI) (mean ± SEM, n = 5). **H**, Quantification of CD68^{+} cells in the cap and core region of atherosclerotic plaque as a percent of cells in the region of interest (ROI) (mean ± SEM, n = 5). Scale is 100 μm.

Table 2
Body weight (g) and plasma lipids levels (mg/dL) in *Apoe*$^{-/-}$ mice with SMC-specific *Noxa1* deletion after 12 weeks of Western diet. Data are mean ± SEM, n = 10.

	Noxa1$^{flox/flox}$/*Apoe*$^{-/-}$	SM22α-CreKI/*Apoe*$^{-/-}$	*Noxa1*$^{SMC-/-}$/*Apoe*$^{-/-}$
Body weight	31.9 ± 0.9	32.8 ± 1.4	33.6 ± 1.4
Cholesterol	778 ± 39.2	817.5 ± 52.1	852.1 ± 60.9
Triglycerides	176.5 ± 12.7	202.1 ± 7.3	187.5 ± 17.1

For this, we first measured superoxide and hydrogen peroxide generation. TNFα induced a 175% increase in CM-H_2DCFDA fluorescence in the wild-type VSMC, which was abrogated by pretreatment with diphenyliodonium (DPI), a non-specific inhibitor of flavin-containing enzymes (Fig. 5A). In contrast, TNFα had no significant effect on H_2DCFDA fluorescence in *Noxa1*$^{SMC-/-}$ cells. Similarly, superoxide levels, determined by HPLC analysis of dihydroxyethidium oxidation, were significantly increased in TNFα-treated (210%) wild-type but not *Noxa1*$^{SMC-/-}$ cells (30%) and were inhibited by pretreatment with DPI (Fig. 5B). TNFα also significantly increased hydrogen peroxide levels as measured by Amplex Red assay in the wild-type cells ($P < 0.01$), but had no such effect in *Noxa1*-deficient cells (Fig. 5C). Notably, there was

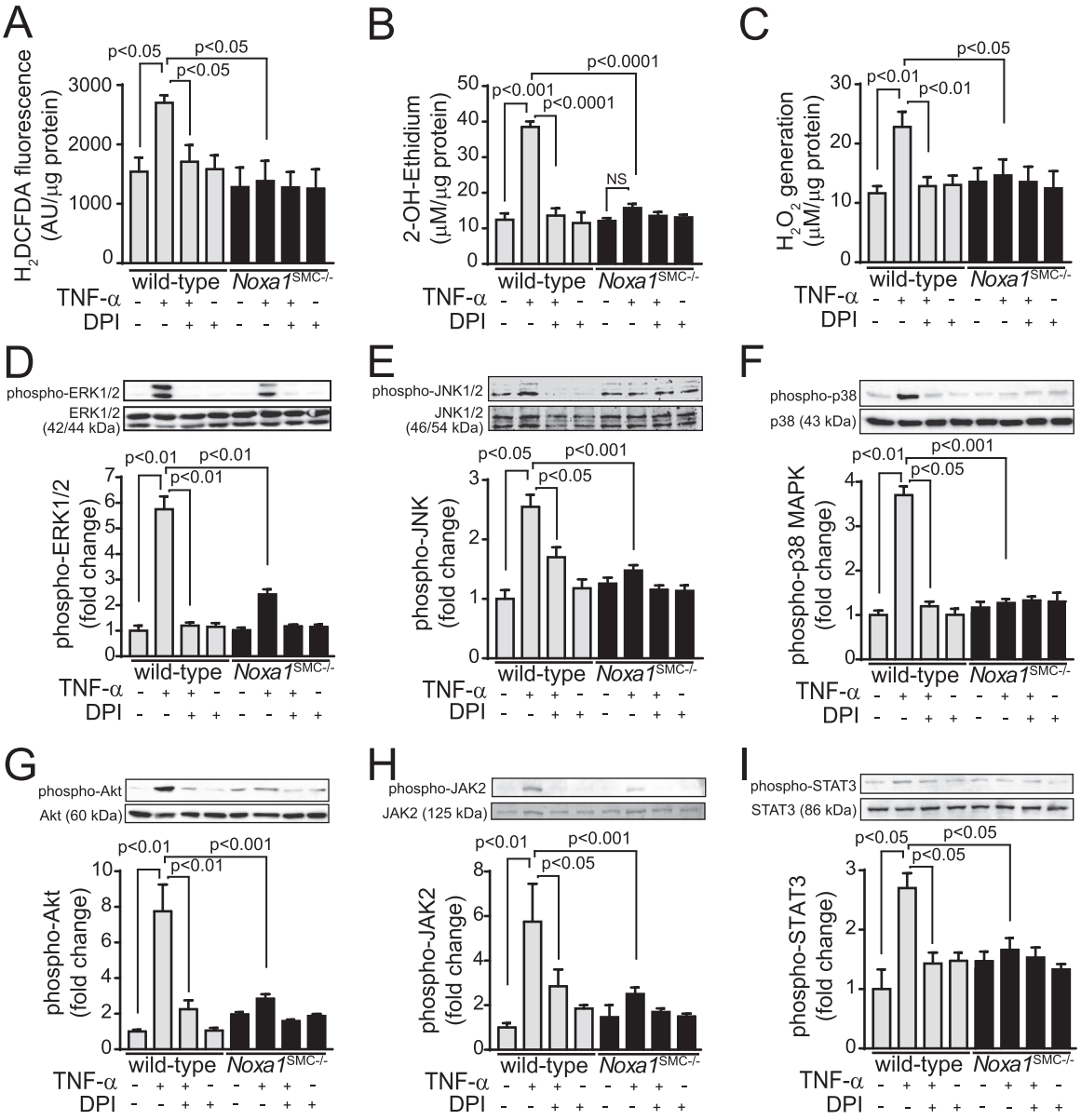

Fig. 5. *Noxa1* deficiency significantly attenuates TNFα-induced ROS generation and suppresses redox-sensitive protein kinase activation in VSMC. A, ROS levels were determined in VSMC treated with 100 ng/ml TNFα for 10 min with or without 10 μM DPI by measuring H_2DCFDA fluorescence. B, Superoxide generation in VSMC treated with 100 ng/ml TNFα for 10 min with and without 10 μM DPI was measured by 2-OH-ethidium HPLC analysis. C, Hydrogen peroxide levels in VSMC treated with 100 ng/ml TNFα for 10 min with and without 10 μM DPI were measured by Amplex Red assay. Data in A-C were normalized to protein concentration and are mean ± SEM, n = 4. D-I, Western blot analysis of phosphorylated ERK1/2 (D), JNK (E), p38 (F), Akt (G), JAK2 (H), and STAT3 (I) protein levels in VSMC treated with 100 ng/ml TNFα for 10 min in the presence and absence of 10 μM DPI. Western blot densitometry analysis presented as mean ± SEM (n = 4) of fold change in phosphoprotein levels adjusted for total protein levels.

no significant difference in basal ROS levels between the wild-type and *Noxa1*$^{SMC-/-}$ cells, suggesting that NOXA1 is a critical regulator of TNFα-induced ROS generation in VSMC.

Next, we measured redox-sensitive protein kinase activation in VSMC from the wild-type and *Noxa1*$^{SMC-/-}$ mice. Western blot analysis of TNFα-treated cell lysates showed a significant increase in ERK1/2 threonine and tyrosine phosphorylation at 10 min in the wild-type cells (5.7-fold increase; $P < 0.01$), which was abrogated by DPI pretreatment (Fig. 5D). In contrast, TNFα-induced ERK1/2 phosphorylation was significantly attenuated in *Noxa1*$^{SMC-/-}$ cells. TNFα significantly stimulated JNK1/2 threonine and tyrosine phosphorylation (2.5-fold increase) 10 min after TNFα treatment in the wild-type, which was inhibited by DPI (Fig. 5E). Similarly, p38 MAPK threonine and tyrosine phosphorylation was markedly increased in the wild-type cells after the treatment (3.7-fold increase; $P < 0.01$), which was sensitive to inhibition by DPI (Fig. 5F). TNFα had no stimulatory effect on JNK1/2 and p38 MAPK phosphorylation in *Noxa1*$^{SMC-/-}$ cells. Akt serine phosphorylation was increased by 7.8-fold in the wild-type VSMC treated with TNFα for 10 min ($P < 0.01$; Fig. 5G); TNFα stimulated Akt phosphorylation was markedly inhibited by DPI pretreatment, while the cytokine failed to stimulate Akt phosphorylation in *Noxa1*$^{SMC-/-}$ cells. JAK2 and STAT3 tyrosine phosphorylation were increased by 5.8- and 2.7-fold, respectively, after TNFα treatment in the wild-type cells, while DPI pretreatment noticeably inhibited this effects (Figs. 5H and 5I). TNFα had no marked effect on JAK2 and STAT3 phosphorylation in *Noxa1*$^{SMC-/-}$ cells.

The sterile-20-like mitogen activated protein kinase kinase kinase kinase 4 (MAP4K4) is reported to mediate TNFα-induced inflammatory effects in various cell types and promote atherogenesis in *Apoe*$^{-/-}$ and *Ldlr*$^{-/-}$ mice [36,37]. Congruent with these data, MAP4K4 expression

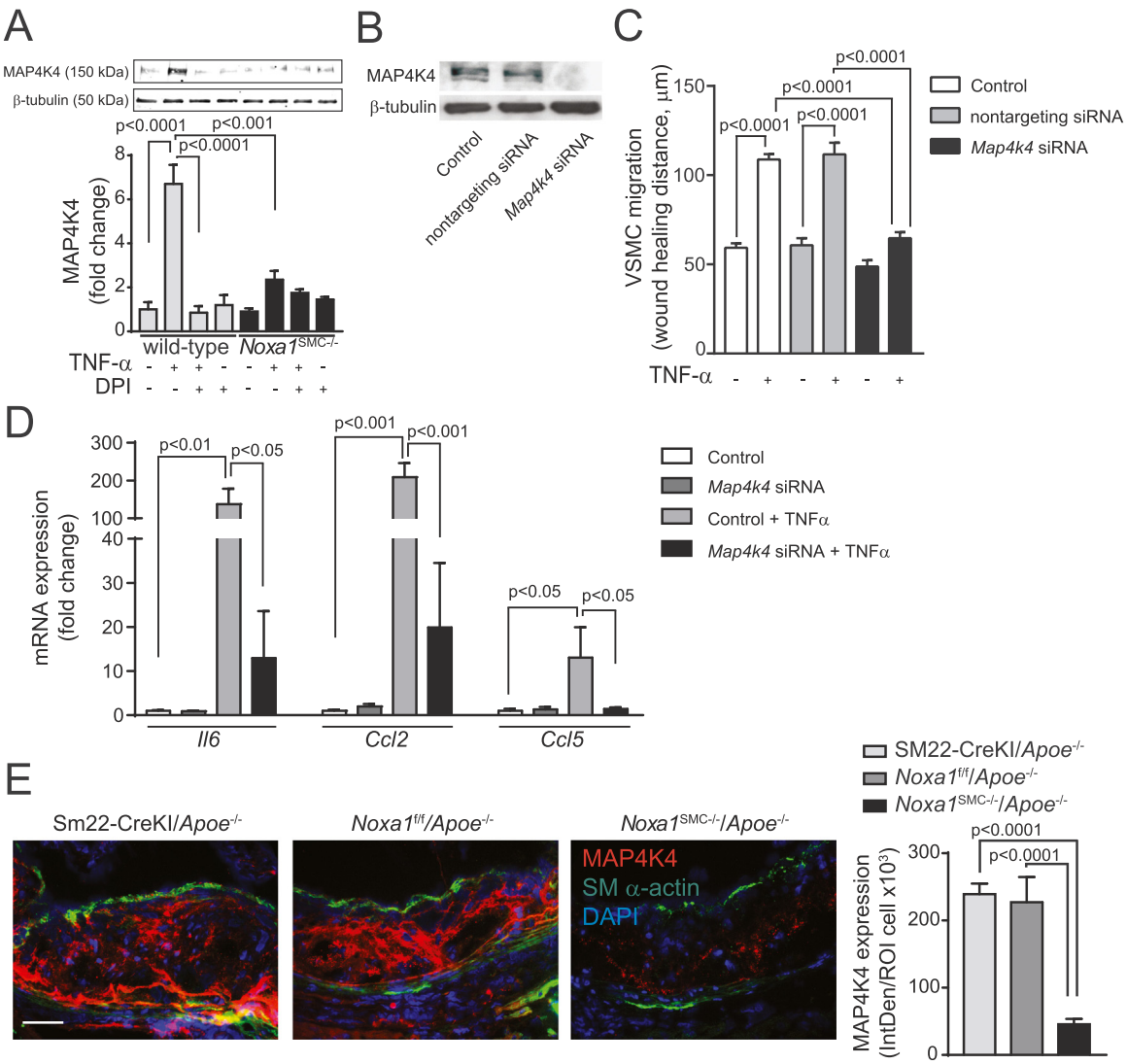

Fig. 6. MAP4K4 expression is correlated with TNFα-induced VSMC migration, proinflammatory gene expression and atherosclerotic lesion size in *Noxa1*$^{SMC-/-}$/*Apoe*$^{-/-}$ mice. A, Western blot analysis of MAP4K4 protein levels in cells treated with 100 ng/ml TNFα for 6 h with and without 10 μM DPI. Densitometry analysis of MAP4K4 normalized to β-tubulin levels (mean ± SEM; n = 4). B, Western blot analysis of MAP4K4 protein levels in VSMC untransfected and transfected with nontargeting or *Map4k4* siRNA. C, VSMC migration assessed by scratch wound assay in cells untransfected and transfected with nontargeting or *Map4k4* siRNA in the presence and absence of 100 ng/ml TNFα for 24 h. Maximal wound healing distance is presented (mean ± SEM; n = 3). D, Relative mRNA expression levels as assessed by real time-PCR (mean ± SEM, n = 4). E, Representative immunofluorescence images and quantification of aortic root sections stained for MAP4K4 (red), SM-α-actin (green) and with DAPI (blue). Data presented as integrated density of fluorescence per number of cells (mean ± SEM, n = 6). Scale is 100 μm.

was significantly induced in the wild-type VSMC 6 h after TNFα treatment (6.7-fold increase), an effect that was suppressed by DPI pretreatment (Fig. 6A). TNFα had no significant effect on MAP4K4 expression in *Noxa1*$^{SMC-/-}$ cells. To determine whether modulation of MAP4K4 expression levels affects functional activation of VSMC we transfected the cells with nontargeting or *Map4k4* siRNA. Transfection with *Map4k4* siRNA markedly reduced MAP4K4 protein levels compared to nontargeting siRNA (Fig. 6B). Treatment with TNFα significantly induced cell migration in non-transfected control or nontargeting siRNA transfected VSMC but abrogated it in *Map4k4* siRNA transfected cells (Fig. 6C). Additionally, TNFα significantly increased expression of proinflammatory genes *Il6*, *Ccl2* and *Ccl5* in control VSMC, which was attenuated in *Map4k4* siRNA transfected VSMC (Fig. 6D). Immunofluorescence analysis of atherosclerotic plaque sections demonstrated that MAP4K4 protein expression was majorly localized to necrotic core and medial SMC and was significantly reduced in the lesions of *Noxa1*$^{SMC-/-}$/*Apoe*$^{-/-}$ compared with control *Apoe*$^{-/-}$ mice (Fig. 6E). These results suggest that increased NOXA1 expression under hyperlipidemic conditions enhances atherosclerosis, in part, by inducing SMC migration and proinflammatory gene expression via enhanced MAP4K4 expression. Taken together, these data show that NOXA1-dependent NADPH oxidase is a critical regulator of inflammatory agonist-induced ROS generation and activation of downstream protein kinases involved in proliferation and migration of aortic SMC, intraplaque inflammation and atherosclerotic lesion expansion.

3.6. Smooth muscle-specific deletion of Noxa1atenuates VSMC phenotypic modulation in atherosclerosis

VSMC exhibit remarkable plasticity in response to environmental stimuli such as increased oxidative stress, undergoing contractile to synthetic phenotype transition [38]. However, recent evidence extends VSMC plasticity to transdifferentiation into macrophage-like cells during atherogenesis that is dependent on KLF4, a transcription factor that induces VSMC dedifferentiation [25,39]. In addition, high TNFα and oxLDL levels present in the inflammatory milieu of atherosclerotic

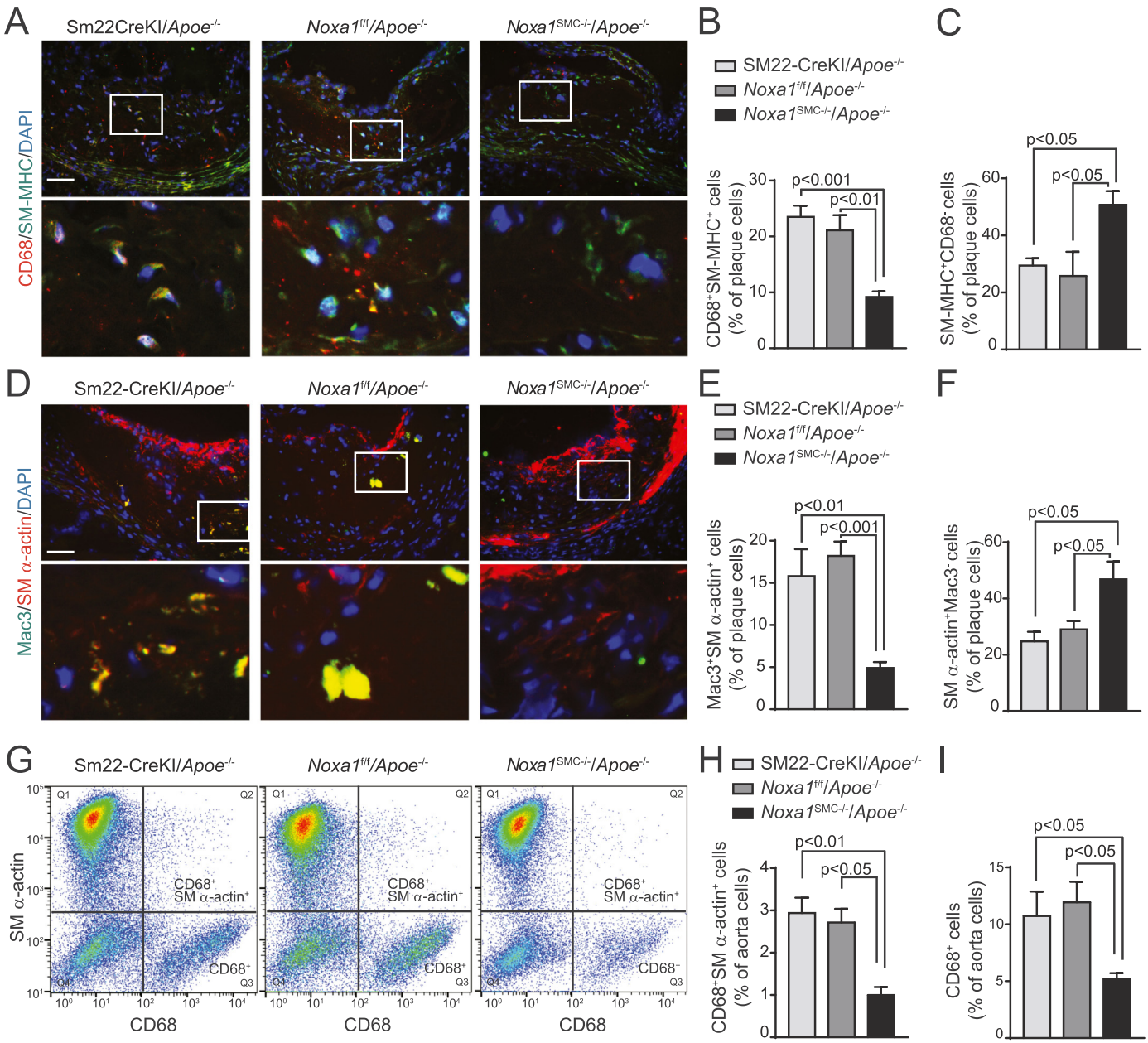

Fig. 7. Increased presence of SMC expressing macrophage markers in atherosclerotic lesions from *Apoe*$^{-/-}$ but not *Noxa1*$^{SMC-/-}$/*Apoe*$^{-/-}$ mice. A, Representative immunofluorescence images of aortic root sections stained for CD68 (red), SM-MHC (green) and with DAPI (blue). Scale is 100 μm. Higher magnification of insets (white rectangles) are in the lower panel. B, Quantification of CD68$^+$ and SM-MHC$^+$ dual marker plaque cells (mean ± SEM, n = 6). C, Quantification of SM-MHC$^+$ and CD68$^-$ plaque cells (mean ± SEM, n = 6). D, Representative immunofluorescence images of aortic root sections stained for Mac3 (green), SM-α-actin (red) and counterstained with DAPI (blue). Higher magnification of insets (white rectangles) are in the lower panel. E, Quantification of Mac3$^+$ and SM-α-actin$^+$ dual marker plaque cells (mean ± SEM, n = 6). F, Quantification of SM-MHC$^+$ and Mac3$^-$ plaque cells (mean ± SEM, n = 6). G, Flow cytometry analysis of whole aorta single cell suspension for CD68$^+$ and SM-α-actin$^+$ dual-labeled cells. H, Flow cytometry quantification of CD68$^+$ and SM-α-actin$^+$ dual-labeled cell fraction of whole aorta (mean ± SEM, n = 4). I, Flow cytometry quantification of CD68$^+$ cell fraction of whole aorta (mean ± SEM, n = 4).

lesions simulate KLF4 expression in VSMC [40,41]. Therefore, we investigated whether the decreased atherosclerotic burden *in Noxa1*$^{SMC-/-}$/*Apoe*$^{-/-}$ versus *Apoe*$^{-/-}$ mice is mediated, in part, by attenuated KLF4 expression and VSMC transdifferentiation. Compared with *Apoe*$^{-/-}$ mice, atherosclerotic plaques from *Noxa1*$^{SMC-/-}$/*Apoe*$^{-/-}$ mice had a significantly lower fraction of cells positive for both macrophage marker CD68 and smooth muscle myosin heavy chain (SM-MHC), as determined by immunofluorescent staining (22% versus 9%; Fig. 7A-B). In contrast, the fraction of plaque cells stained for SM-MHC but not CD68 was significantly higher in *Noxa1*$^{SMC-/-}$/*Apoe*$^{-/-}$ compared with *Apoe*$^{-/-}$ mice (51% and 28%, respectively; Fig. 7C), suggesting that lower number of plaque SMC was undergoing phenotypic transition in *Noxa1*-deficient mice. Similarly, the fraction of cells positive for macrophage marker Mac3 and SMC α-actin was also significantly lower (5% versus 17%; Fig. 7D-E), whereas the fraction of α-actin$^+$ cells not stained for Mac3 was higher (47% versus 27%; Fig. 7F) in the atherosclerotic lesions of *Noxa1*$^{SMC-/-}$/*Apoe*$^{-/-}$ compared with *Apoe*$^{-/-}$ mice. The macrophage-like cells expressing dual markers were primarily localized to the necrotic core area, indicating SMC transdifferentiation occurred on exposure to oxidized phospholipids. Congruent with that, flow cytometry analysis of cell suspension from atherosclerotic aortas confirmed the presence of dual marker cells (Fig. 7G) and significantly lower levels of dual labeled CD68$^+$ α-actin$^+$ cells in aortas of *Noxa1*$^{SMC-/-}$/*Apoe*$^{-/-}$ versus *Apoe*$^{-/-}$ mice (1% and 2.8% of total cells,

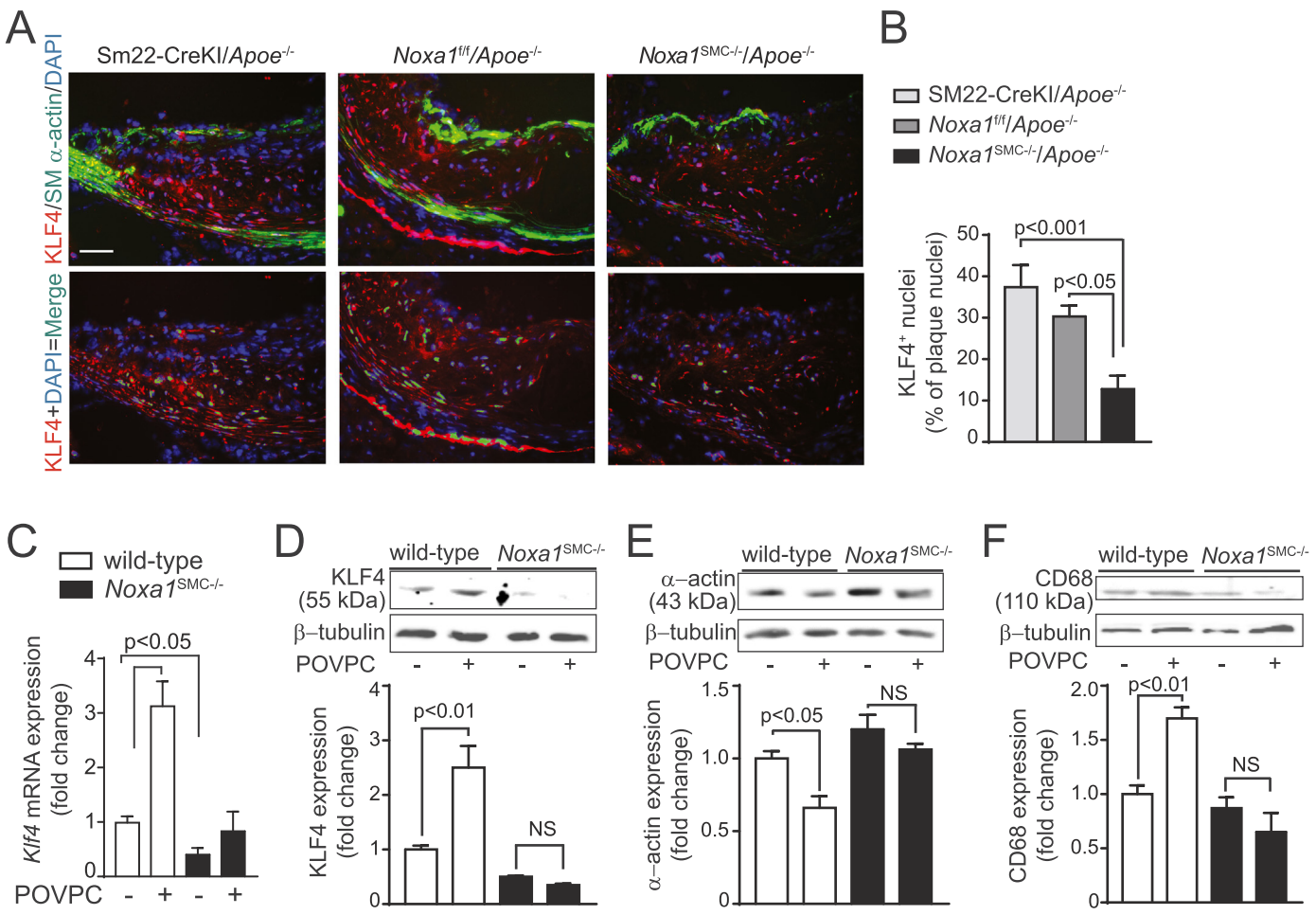

Fig. 8. *Noxa1* deficiency attenuates KLF4 expression and nuclear localization in aortic atherosclerotic lesion cells of *Apoe*$^{-/-}$ mice and expression in VSMC exposed to oxidized phospholipids. A, Representative immunofluorescence images of aortic root sections stained for KLF4 (red), SM-α-actin (green) and with DAPI (blue) (upper panel). Colocalization of KLF4 (red) and nuclear DAPI (blue) in atherosclerotic lesions were pseudocolored green (lower panel). Scale is 100 μm. B, Quantification of KLF4-positive (green) nuclei as a fraction of all nuclei (mean ± SEM, n = 6). C, RT-PCR analysis of *Klf4* mRNA expression in VSMC treated with POVPC for 4 h. D-F, Western blot analysis of KLF4 (D), SM-α-actin (E), and CD68 (F) expression in VSMC treated with POVPC for 24 h. Densitometry analysis of respective proteins normalized to β-tubulin levels (mean ± SEM; n = 4).

respectively; Fig. 7H). In addition, the percent of CD68^{+} cells were significantly lower in whole aorta single cell suspensions from *Noxa1*$^{SMC-/-}$/*Apoe*$^{-/-}$ compared with *Apoe*$^{-/-}$ mice (Fig. 7I), reflecting lower atherosclerotic lesion area (Fig. 4C).

The expression and nuclear localization of KLF4 was markedly reduced in the atherosclerotic lesions of *Noxa1*$^{SMC-/-}$/*Apoe*$^{-/-}$ compared with control *Apoe*$^{-/-}$ mice (13% versus 35%; Fig. 8A-B). Notably, cells with KLF4^{+} nuclei (KLF4 and DAPI colocalization) were largely present in the media and necrotic core area of the plaque, suggesting the medial SMC as a source of the plaque macrophage-like cells. Oxidized phospholipids, including POVPC, were shown to induce KLF4-dependent phenotypic changes in VSMC [42]. Accordingly, 4 h POVPC treatment of VSMC isolated from wild-type mice resulted in significant induction of *Klf4* mRNA. Expression of *Klf4* was significantly lower in *Noxa1*$^{SMC-/-}$ cells and treatment with POVPC did not changed its expression (Fig. 8C). In concert with that, expression of KLF4 protein was significantly increased by POVPC treatment in wild-type but not in *Noxa1*$^{SMC-/-}$ cells (Fig. 8D). The expression of SM α-actin decreased (Fig. 8E) while the expression of CD68 protein increased (Fig. 8F) significantly after POVPC treatment in the wild-type but not in *Noxa1*$^{SMC-/-}$ cells. These results suggest that SMC-specific NOXA1-dependent NADPH oxidase regulates the phenotypic fate of the SMC in the pro-oxidant environment of atherosclerotic plaque.

3.7. NADPH oxidase-dependent SMC phenotypic transition enhanced intraplaque inflammation

VSMC-derived atherosclerotic plaque cells exhibit pro-inflammatory phenotype and contribute to vessel wall remodeling [23,25,43]. In line with this, RNA expression of monocyte chemotactic protein 1 (*Ccl2*), vascular cell adhesion molecule 1 (*Vcam1*), and matrix metalloproteinase 2 (*Mmp2*) was significantly increased in wild-type VSMC after treatment with POVPC but in *Noxa1*$^{SMC-/-}$ cells (Fig. 9A). In addition, immunofluorescence analysis of aortic root transverse sections showed markedly reduced expression of immunoreactive VCAM1 protein in the SM α-actin^{+} cells in atherosclerotic lesions of *Noxa1*$^{SMC-/-}$/*Apoe*$^{-/-}$ compared with *Apoe*$^{-/-}$ mice (Fig. 9B). Notably, the cells expressing VCAM1 were largely present in the necrotic core area and on the border with fibrous cap. Expression of immunoreactive CCL2 in atherosclerotic lesions was also significantly reduced in *Noxa1*$^{SMC-/-}$/*Apoe*$^{-/-}$ compared with *Apoe*$^{-/-}$ mice (Fig. 9C). The SM α-actin^{+} cells expressing CCL2 were primarily present in the medial and fibrous cap regions of the atherosclerotic plaques from *Apoe*$^{-/-}$ mice. The MMP2 expression was strongest in the core area while SM α-actin^{+} cells expressing MMP2 were detected in the media of *Apoe*-deficient mice. Expression of immunoreactive MMP2 was significantly lower in the atherosclerotic lesions of *Noxa1*$^{SMC-/-}$/*Apoe*$^{-/-}$ mice (Fig. 9D). These results support the role of NOXA1-based NADPH oxidase-dependent ROS generation in

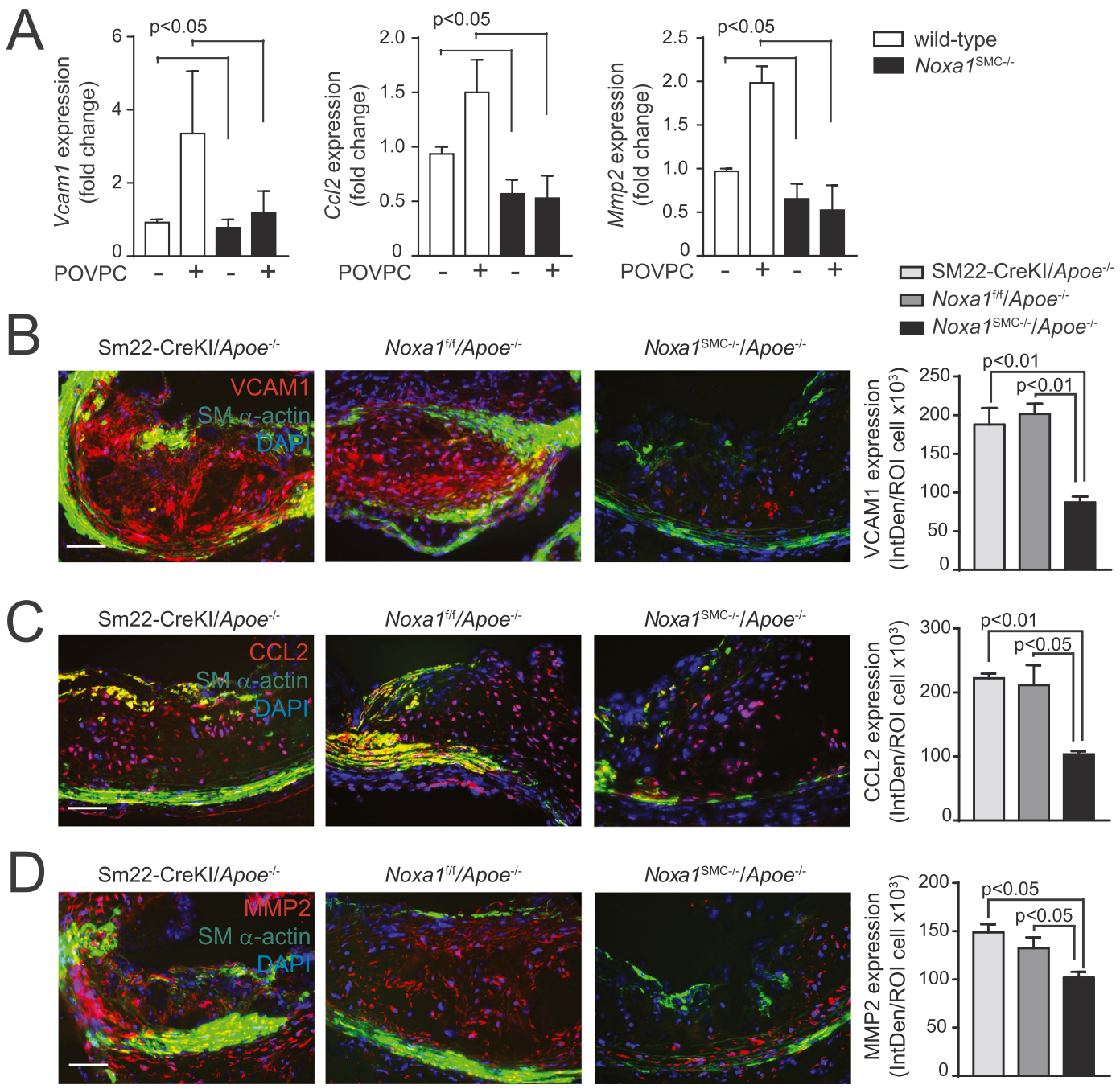

Fig. 9. Expression of proteins downstream of KLF4 is reduced in VSMC from *Noxa1*$^{SMC-/-}$ versus wild-type mice and in atherosclerotic lesions from *Noxa1*$^{SMC-/-}$*/Apoe*$^{-/-}$ versus *Apoe*$^{-/-}$ mice. A, Real time PCR analysis of *Vcam1*, *Ccl2*, and *Mmp2* mRNA expression levels in VSMC treated with POVPC for 24 h. B-D, Representative immunofluorescence images and quantification of aortic root sections stained for VCAM1 (B), CCL2 (C) and MMP2 (D) (red), costained for SM-α-actin (green), and with DAPI (blue). Data presented as integrated density of fluorescence per number of cells (mean ± SEM, n = 4). Scale is 100 μm.

enhanced intraplaque inflammation, plaque core expansion and matrix remodeling.

4. Discussion

In the current study we utilized novel global and VSMC-specific *Noxa1* knockout mouse models to test the hypothesis that NOXA1-dependent NADPH oxidase is an important regulator of VSMC function in pathophysiological conditions during arterial restenosis and atherosclerosis development. The central tenet that aberrant proliferation of VSMC promotes atherosclerotic plaque formation whereas VSMC in advanced lesions support plaque stability and the preponderance of macrophages and macrophage-derived foam cells relative to VSMC within the fibrous cap and shoulder regions increases plaque vulnerability is, in fact, too simplistic to describe the various processes VSMC undergo during atherogenesis and plaque progression and greatly underestimates the contribution of VSMC to the pathogenesis of atherosclerosis [25,43]. Supporting this concept, our data show that dysregulation of VSMC plasticity and physiology under hyperlipidemic conditions increases atherosclerotic burden; VSMC-specific NOXA1-dependent NOX1 NADPH oxidase activation is a critical regulator of the pathogenesis and progression of atherosclerosis.

In line with previous results using *Nox1*$^{-/y}$ mice [7] and our in vivo data showing increased neointimal thickness with localized

overexpression of NOXA1 in injured carotid arteries [20], *Noxa1* gene deletion reduced arterial neointimal hyperplasia and outward remodeling. Supporting this observation, TNFα-induced ROS levels and protein kinase activation were attenuated and cell migration and proliferation were reduced in *Noxa1*$^{-/-}$ VSMC. In addition to cell proliferation and migration [44], oxidative stress-dependent activation of ERK1/2 and p38 MAPK kinases promotes atherosclerosis by inducing expression of inflammatory genes such as *Ccl2* [45,46]. Similarly, activation of JNK1 in VSMC by vasoactive agonists stimulates VCAM-1 expression and inflammation [47] and Akt activation induces VSMC dedifferentiation and osteogenic transition via enhanced expression and activity of RUNX2, resulting in atherosclerotic lesion calcification [48]. The JAK2-STAT3 pathway activation also contributes to atherosclerosis; a JAK2 inhibitor, AG490, markedly reduced the expression of NOX1, NOX2 and NOX4 and lesion area in *Apoe*$^{-/-}$ mice [49] and immunoreactive activated STAT3 was observed in human atherosclerotic lesions and endothelial-specific *Stat3*$^{-/-}$ mice had reduced fatty streak formation [50]. Our data showing NOXA1-dependent regulation of MAP4K4 expression in VSMC and atherosclerotic lesions is in line with its role in promoting MAP kinase activation, inflammatory cytokine and adhesion molecule expression, and cell migration as well as atherosclerosis in hyperlipidemic mice [37].

Our previous data from allogenic, sex-mismatched bone marrow transplantation studies showed that NADPH oxidase activation in both monocyte/macrophages and vessel wall cells plays a critical role in atherosclerosis [15]. The current data showing a significant reduction in aortic atherosclerosis in Apoe$^{-/-}$ mice by attenuation of NADPH oxidase activity in VSMC underscores the important contribution of VSMC to atherogenesis and plaque progression. The reduction in atherosclerotic burden under hyperlipidemic conditions with decreased oxidative stress is achieved by attenuating not only VSMC activation as measured by proliferation, migration, and proinflammatory molecule expression, but also VSMC population of atherosclerotic plaque core region and transition to macrophage-like cells. Supporting the major contribution of VSMC to atherosclerotic plaque pathogenesis, lineage tracing studies showed that attenuation of VSMC phenotypic transition to macrophage-like cells has significant beneficial effect on plaque size and stability [25].

Furthermore, lineage studies showed that a majority of SMC in hyperlipidemia-induced atherosclerotic lesions originate from the medial layer of the vessel wall and not derived from the bone marrow progenitor cells [51,52]. Similarly, a large fraction of Mac2$^+$ cells within atherosclerotic lesions of Western diet fed *Apoe*$^{-/-}$ mice were not derived from hematopoietic cells [50,51]. Supporting this notion and underscoring the clinical relevance of SMC phenotypic switch, Allahverdian et al. [53] reported that only ~35% of the CD68$^+$ cells in human coronary atherosclerotic lesions were positive for the leukocyte marker CD45 which means that a large portion of macrophages in atherosclerotic lesions are not of the myeloid lineage; costaining studies showed that ~40% of CD68$^+$ cells and ~50% foam cells in advanced lesions were SMC-derived. Likewise, lineage-tracing studies showed that VSMC-derived cells constitute ~30% and ~20% of core cells and shoulder region cells, respectively, in atherosclerotic lesions of *Apoe*$^{-/-}$ mice [43]. Our data showing ~20% of VSMC-derived macrophage-like cells in atherosclerotic lesions may be an underestimate and represent limitation of staining for traditional SMC markers as Owens and colleagues report that ~82% of SMC within the lesions are ACTA2 negative [25]. Coupled with this, significant reduction of the number of CD68/Mac3$^+$ SMC in the plaques of *Noxa1*$^{SMC-/-}$/*Apoe*$^{-/-}$ mice suggests that NOXA1-dependent ROS is a major contributor to phenotypic transition of SMC, without directly affecting the phenotype of bone marrow-derived cells.

Our results suggest that SMC phenotypic switch is largely regulated by KLF4 which is not expressed in differentiated VSMC, but can be induced by oxidized phospholipids and inflammatory cytokines, downregulating expression of SMC markers while inducing expression of macrophage- and mesenchymal cell-like markers [25,54]. Lending support to this notion, Starke et al. [38] recently showed that increased NOX1 expression and enhanced ROS levels in cerebral VSMC exposed to cigarette smoke were followed by upregulation of proinflammatory/matrix remodeling genes including *Klf4* and down regulation of contractile genes SM-α-actin, SM-22α, SM-MHC and myocardin, effects which were reversed by the inhibition of ROS and knockdown of NOX1. Indeed, our data show that plaque cells expressing dual SMC/macrophage markers are localized to the oxidized lipids-rich core area where increased expression of KLF4 was evident. This is in line with our previous results, showing association of increased oxidative stress with greater number of SMC-derived macrophage-like cells in the core, whose apoptosis causes expansion of the core in advanced lesions [22]. In this context, it is noteworthy that oxidized phospholipid induced SMC phenotypic modulation was attenuated by siRNA targeting of *Klf4* and in *Klf4* knockout SMC [41]. Congruent with this, *Apoe*$^{-/-}$ with SMC-specific conditional knockout of *Klf4* had decreased number of SMC-derived macrophage-like cells, reduced atherosclerotic burden and stable plaque phenotype, including increase in fibrous cap thickness, compared with *Apoe*$^{-/-}$ mice [25]. In agreement, our data show a positive correlation between reduced intraplaque SMC KLF4 expression and attenuated atherosclerosis in *Noxa1*$^{SMC-/-}$/*Apoe*$^{-/-}$ versus *Apoe*$^{-/-}$ mice. Interestingly, *Map4k4* was also identified as one of the SMC-specific KLF4 transcriptional targets [25].

However, the effects of KLF4 on atherosclerosis may be cell-type dependent as myeloid- or endothelial cell-specific deletion of *Klf4* augmented atherosclerosis and plaque inflammatory cell accumulation in *Apoe*$^{-/-}$mice [55,56]. In addition to oxidative stress, *Klf4* expression is also tightly regulated by miRNAs [57] and transcriptional coregulators [54,58]. For example, the knockout of miR-143/145, negative regulators of *Klf4*, reduced early neointimal lesions [59], whereas SMC-specific overexpression of miR-145 reduced KLF4 levels and plaque size in *Apoe*$^{-/-}$ mice [60]. Furthermore, it is suggested that cholesterol loading of VSMC downregulates miR-143/145, inducing *Klf4* levels and downregulating SMC markers [61].

NoxA1-dependent NADPH oxidase-derived oxidative stress could affect atherosclerosis by several mechanisms. For instance, SMC-derived cells in human atherosclerotic plaque contain a large burden of excess cholesterol, in part, because of their impaired efflux of cholesterol via ABCA1, whose expression was greatly reduced in advanced lesions [53]. The decrease in ABCA1 expression might be mediated by oxidative stress as inflammatory cytokines reduce its expression, which is reversed by *N*-acetyl-L-cysteine, a ROS scavenger [62]. VSMC-derived ROS may also affect atherosclerosis through modulation of vascular tone and blood pressure as evident by increased atherosclerotic plaque volume in hypertension subjects [63]. High blood pressure in *Apoe*$^{-/-}$ mice is associated with oxidative stress [64] and angiotensin II-derived vascular ROS are implicated in hypertension that accelerates atherosclerosis [65]. Moreover, recent studies found that *Nox1*$^{-/y}$ had significantly lower [66] whereas mice with SMC-specific overexpression of *Nox1* had higher blood pressure in response to angiotensin II treatment [67]. Our results suggest that NOXA1, because its expression is quickly induced by TNFα and angiotensin II [20], may act as a primary regulator of NOX1 hyperactivation in VSMC, supporting its critical role in regulation of hypertension, vascular inflammation, restenosis, and atherosclerosis.

Recent reports of the successful targeting of NADPH oxidase using dual NOX1/NOX4 inhibitors [16,18] provides evidence for the potential role of NOX1-derived ROS in the pathogenesis of atherosclerosis; however, many NOX inhibitors lack molecular and cellular specificity. Our results support the notion that selective inhibition of SMC-specific NOX1, by inhibiting NOXA1 interaction with p47phox, may be an effective therapeutic approach in CVD treatment.

Acknowledgments

None.

Funding

This work was supported by the National Institutes of Health, USA grants HL111664 and HL139842.

Disclosures

None.

References

[1] P. Libby, Inflammation in atherosclerosis, Arterioscler. Thromb. Vasc. Biol. 32 (2012) 2045–2051.
[2] N.R. Madamanchi, M.S. Runge, Mitochondrial dysfunction in atherosclerosis, Circ. Res. 100 (2007) 460–473.
[3] N.R. Madamanchi, M.S. Runge, Redox signaling in cardiovascular health and disease, Free Radic. Biol. Med. 61 (2013) 473–501.
[4] B. Lassegue, A. San Martin, K.K. Griendling, Biochemistry, physiology, and pathophysiology of NADPH oxidases in the cardiovascular system, Circ. Res. 110 (2012) 1364–1390.
[5] A. Konior, A. Schramm, M. Czesnikiewicz-Guzik, T.J. Guzik, NADPH oxidases in vascular pathology, Antioxid. Redox Signal. 20 (2014) 2794–2814.
[6] L. Serrander, L. Cartier, K. Bedard, B. Banfi, B. Lardy, O. Plastre, A. Sienkiewicz, L. Forro, W. Schlegel, K.H. Krause, Nox4 activity is determined by mRNA levels and reveals a unique pattern of ros generation, Biochem. J. 406 (2007) 105–114.
[7] M.Y. Lee, A. San Martin, P.K. Mehta, A.E. Dikalova, A.M. Garrido, S.R. Datla, E. Lyons, K.H. Krause, B. Banfi, J.D. Lambeth, B. Lassegue, K.K. Griendling, Mechanisms of vascular smooth muscle NADPH oxidase 1 (Nox1) contribution to injury-induced neointimal formation, Arterioscler. Thromb. Vasc. Biol. 29 (2009) 480–487.
[8] I. Szanto, L. Rubbia-Brandt, P. Kiss, K. Steger, B. Banfi, E. Kovari, F. Herrmann, A. Hadengue, K.H. Krause, Expression of Nox1, a superoxide-generating NADPH oxidase, in colon cancer and inflammatory bowel disease, J. Pathol. 207 (2005) 164–176.
[9] C. Cheret, A. Gervais, A. Lelli, C. Colin, L. Amar, P. Ravassard, J. Mallet, A. Cumano, K.H. Krause, M. Mallat, Neurotoxic activation of microglia is promoted by a Nox1-dependent NADPH oxidase, J. Neurosci. 28 (2008) 12039–12051.
[10] J.S. Kim, S. Yeo, D.G. Shin, Y.S. Bae, J.J. Lee, B.R. Chin, C.H. Lee, S.H. Baek, Glycogen synthase kinase 3beta and beta-catenin pathway is involved in toll-like receptor 4-mediated NADPH oxidase 1 expression in macrophages, FEBS J. 277 (2010) 2830–2837.
[11] Q. Xu, S. Choksi, J. Qu, J. Jang, M. Choe, B. Banfi, J.F. Engelhardt, Z.G. Liu, NADPH oxidases are essential for macrophage differentiation, J. Biol. Chem. 291 (2016) 20030–20041.
[12] K. Szocs, B. Lassegue, D. Sorescu, L.L. Hilenski, L. Valppu, T.L. Couse, J.N. Wilcox, M.T. Quinn, J.D. Lambeth, K.K. Griendling, Upregulation of nox-based NAD(P)H oxidases in restenosis after carotid injury, Arterioscler. Thromb. Vasc. Biol. 22 (2002) 21–27.
[13] S. Xu, A.S. Shriver, D.K. Jagadeesha, A.H. Chamseddine, K. Szocs, N.L. Weintraub, K.K. Griendling, R.C. Bhalla, F.J. Miller Jr., Increased expression of Nox1 in neointimal smooth muscle cells promotes activation of matrix metalloproteinase-9, J. Vasc. Res. 49 (2012) 242–248.
[14] A.E. Vendrov, N.R. Madamanchi, Z.S. Hakim, M. Rojas, M.S. Runge, Thrombin and NAD(P)H oxidase-mediated regulation of CD44 and BMP4-Id pathway in VSMC, restenosis, and atherosclerosis, Circ. Res. 98 (2006) 1254–1263.
[15] A.E. Vendrov, Z.S. Hakim, N.R. Madamanchi, M. Rojas, C. Madamanchi, M.S. Runge, Atherosclerosis is attenuated by limiting superoxide generation in both macrophages and vessel wall cells, Arterioscler. Thromb. Vasc. Biol. 27 (2007) 2714–2721.
[16] A.E. Vendrov, N.R. Madamanchi, X.L. Niu, K.C. Molnar, M. Runge, C. Szyndralewiez, P. Page, M.S. Runge, NADPH oxidases regulate CD44 and hyaluronic acid expression in thrombin-treated vascular smooth muscle cells and in atherosclerosis, J. Biol. Chem. 285 (2010) 26545–26557.
[17] A.L. Sheehan, S. Carrell, B. Johnson, B. Stanic, B. Banfi, F.J. Miller Jr., Role for Nox1 NADPH oxidase in atherosclerosis, Atherosclerosis 216 (2011) 321–326.
[18] S.P. Gray, E. Di Marco, J. Okabe, C. Szyndralewiez, F. Heitz, A.C. Montezano, J.B. de Haan, C. Koulis, A. El-Osta, K.L. Andrews, J.P. Chin-Dusting, R.M. Touyz, K. Wingler, M.E. Cooper, H.H. Schmidt, K.A. Jandeleit-Dahm, NADPH oxidase 1 plays a key role in diabetes mellitus-accelerated atherosclerosis, Circulation 127 (2013) 1888–1902.
[19] R.K. Ambasta, J.G. Schreiber, M. Janiszewski, R. Busse, R.P. Brandes, Noxa1 is a central component of the smooth muscle nadph oxidase in mice, Free Radic. Biol. Med. 41 (2006) 193–201.
[20] X.L. Niu, N.R. Madamanchi, A.E. Vendrov, I. Tchivilev, M. Rojas, C. Madamanchi, R.P. Brandes, K.H. Krause, J. Humphries, A. Smith, K.G. Burnand, M.S. Runge, Nox activator 1: a potential target for modulation of vascular reactive oxygen species in atherosclerotic arteries, Circulation 121 (2010) 549–559.
[21] A.C. Doran, N. Meller, C.A. McNamara, Role of smooth muscle cells in the initiation and early progression of atherosclerosis, Arterioscler. Thromb. Vasc. Biol. 28 (2008) 812–819.
[22] A.E. Vendrov, M.D. Stevenson, S. Alahari, H. Pan, S.A. Wickline, N.R. Madamanchi, M.S. Runge, Attenuated superoxide dismutase 2 activity induces atherosclerotic plaque instability during aging in hyperlipidemic mice, J. Am. Heart Assoc. 6 (2017).
[23] A. Lozhkin, A.E. Vendrov, H. Pan, S.A. Wickline, N.R. Madamanchi, M.S. Runge, NADPH oxidase 4 regulates vascular inflammation in aging and atherosclerosis, J. Mol. Cell Cardiol. 102 (2017) 10–21.
[24] M.R. Bennett, S. Sinha, G.K. Owens, Vascular smooth muscle cells in atherosclerosis, Circ. Res. 118 (2016) 692–702.
[25] L.S. Shankman, D. Gomez, O.A. Cherepanova, M. Salmon, G.F. Alencar, R.M. Haskins, P. Swiatlowska, A.A. Newman, E.S. Greene, A.C. Straub, B. Isakson, G.J. Randolph, G.K. Owens, KLF4-dependent phenotypic modulation of smooth muscle cells has a key role in atherosclerotic plaque pathogenesis, Nat. Med. 21 (2015) 628–637.
[26] J.P. Flaherty, C.A. Spruce, H.E. Fairfield, D.E. Bergstrom, Generation of a conditional null allele of NADPH oxidase activator 1 (NOXA1), Genesis 48 (2010) 568–575.
[27] A.E. Vendrov, K.C. Vendrov, A. Smith, J. Yuan, A. Sumida, J. Robidoux, M.S. Runge, N.R. Madamanchi, Nox4 NADPH oxidase-dependent mitochondrial oxidative stress in aging-associated cardiovascular disease, Antioxid. Redox Signal. 23 (2015) 1389–1409.
[28] J.C. Kovacic, R. Gupta, A.C. Lee, M. Ma, F. Fang, C.N. Tolbert, A.D. Walts, L.E. Beltran, H. San, G. Chen, C. St Hilaire, M. Boehm, Stat3-dependent acute Rantes production in vascular smooth muscle cells modulates inflammation following arterial injury in mice, J. Clin. Investig. 120 (2010) 303–314.
[29] X. Chu, M. Filali, B. Stanic, M. Takapoo, A. Sheehan, R. Bhalla, F.S. Lamb, F.J. Miller Jr., A critical role for chloride channel-3 (cic-3) in smooth muscle cell activation and neointima formation, Arterioscler. Thromb. Vasc. Biol. 31 (2011) 345–351.
[30] A.J. Murphy, M. Akhtari, S. Tolani, T. Pagler, N. Bijl, C.L. Kuo, M. Wang, M. Sanson, S. Abramowicz, C. Welch, A.E. Bochem, J.A. Kuivenhoven, L. Yvan-Charvet, A.R. Tall, Apoe regulates hematopoietic stem cell proliferation, monocytosis, and monocyte accumulation in atherosclerotic lesions in mice, J. Clin. Investig. 121 (2011) 4138–4149.
[31] S. Zadelaar, R. Kleemann, L. Verschuren, J. de Vries-Van der Weij, J. van der Hoorn, H.M. Princen, T. Kooistra, Mouse models for atherosclerosis and pharmaceutical modifiers, Arterioscler. Thromb. Vasc. Biol. 27 (2007) 1706–1721.
[32] T. Skoog, W. Dichtl, S. Boquist, C. Skoglund-Andersson, F. Karpe, R. Tang, M.G. Bond, U. de Faire, J. Nilsson, P. Eriksson, A. Hamsten, Plasma tumour necrosis factor-alpha and early carotid atherosclerosis in healthy middle-aged men, Eur. Heart J. 23 (2002) 376–383.
[33] P. Puz, A. Lasek-Bal, D. Ziaja, Z. Kazibutowska, K. Ziaja, Inflammatory markers in patients with internal carotid artery stenosis, Arch. Med Sci. 9 (2013) 254–260.
[34] N. Xiao, M. Yin, L. Zhang, X. Qu, H. Du, X. Sun, L. Mao, G. Ren, C. Zhang, Y. Geng, L. An, J. Pan, Tumor necrosis factor-alpha deficiency retards early fatty-streak lesion by influencing the expression of inflammatory factors in apoe-null mice, Mol. Genet. Metab. 96 (2009) 239–244.
[35] P.A. Barry-Lane, C. Patterson, M. van der Merwe, Z. Hu, S.M. Holland, E.T. Yeh, M.S. Runge, p47phox is required for atherosclerotic lesion progression in ApoE(-/-) mice, J. Clin. Investig. 108 (2001) 1513–1522.
[36] G.J. Tesz, A. Guilherme, K.V. Guntur, A.C. Hubbard, X. Tang, A. Chawla, M.P. Czech, Tumor necrosis factor alpha (TNFalpha) stimulates Map4k4 expression through TNFalpha receptor 1 signaling to c-Jun and activating transcription factor 2, J. Biol. Chem. 282 (2007) 19302–19312.
[37] R.J. Roth Flach, A. Skoura, A. Matevossian, L.V. Danai, W. Zheng, C. Cortes, S.K. Bhattacharya, M. Aouadi, N. Hagan, J.C. Yawe, P. Vangala, L.G. Menendez, M.P. Cooper, T.P. Fitzgibbons, L. Buckbinder, M.P. Czech, Endothelial protein kinase MAP4K4 promotes vascular inflammation and atherosclerosis, Nat. Commun. 6 (2015) 8995.
[38] R.M. Starke, J.W. Thompson, M.S. Ali, C.L. Pascale, A. Martinez Lege, D. Ding, N. Chalouhi, D.M. Hasan, P. Jabbour, G.K. Owens, M. Toborek, J.M. Hare, A.S. Dumont, Cigarette smoke initiates oxidative stress-induced cellular phenotypic modulation leading to cerebral aneurysm pathogenesis, Arterioscler. Thromb. Vasc. Biol. 38 (2018) 610–621.
[39] Y. Liu, S. Sinha, O.G. McDonald, Y. Shang, M.H. Hoofnagle, G.K. Owens, Kruppel-like factor 4 abrogates myocardin-induced activation of smooth muscle gene expression, J. Biol. Chem. 280 (2005) 9719–9727.
[40] M.S. Ali, R.M. Starke, P.M. Jabbour, S.I. Tjoumakaris, L.F. Gonzalez, R.H. Rosenwasser, G.K. Owens, W.J. Koch, N.H. Greig, A.S. Dumont, TNF-alpha induces phenotypic modulation in cerebral vascular smooth muscle cells: implications for cerebral aneurysm pathology, J. Cereb. Blood Flow. Metab. 33 (2013) 1564–1573.
[41] N.A. Pidkovka, O.A. Cherepanova, T. Yoshida, M.R. Alexander, R.A. Deaton, J.A. Thomas, N. Leitinger, G.K. Owens, Oxidized phospholipids induce phenotypic switching of vascular smooth muscle cells in vivo and in vitro, Circ. Res. 101 (2007) 792–801.
[42] O.A. Cherepanova, N.A. Pidkovka, O.F. Sarmento, T. Yoshida, Q. Gan, E. Adiguzel, M.P. Bendeck, J. Berliner, N. Leitinger, G.K. Owens, Oxidized phospholipids induce type VIII collagen expression and vascular smooth muscle cell migration, Circ. Res. 104 (2009) 609–618.
[43] J. Chappell, J.L. Harman, V.M. Narasimhan, H. Yu, K. Foote, B.D. Simons, M.R. Bennett, H.F. Jorgensen, Extensive proliferation of a subset of differentiated, yet plastic, medial vascular smooth muscle cells contributes to neointimal

formation in mouse injury and atherosclerosis models, Circ. Res. 119 (2016) 1313–1323.
[44] M. Gimenez, B.M. Schickling, L.R. Lopes, F.J. Miller Jr., Nox1 in cardiovascular diseases: regulation and pathophysiology, Clin. Sci. 130 (2016) 151–165.
[45] G.W. De Keulenaer, M. Ushio-Fukai, Q. Yin, A.B. Chung, P.R. Lyons, N. Ishizaka, K. Rengarajan, W.R. Taylor, R.W. Alexander, K.K. Griendling, Convergence of redox-sensitive and mitogen-activated protein kinase signaling pathways in tumor necrosis factor-alpha-mediated monocyte chemoattractant protein-1 induction in vascular smooth muscle cells, Arterioscler. Thromb. Vasc. Biol. 20 (2000) 385–391.
[46] X. Luo, Y. Xiao, F. Song, Y. Yang, M. Xia, W. Ling, Increased plasma S-adenosylhomocysteine levels induce the proliferation and migration of VSMCs through an oxidative stress-ERK1/2 pathway in apoE (-/-) mice, Cardiovasc. Res. 95 (2012) 241–250.
[47] H. Bayat, S. Xu, D. Pimentel, R.A. Cohen, B. Jiang, Activation of thromboxane receptor upregulates interleukin (IL)-1beta-induced VCAM-1 expression through JNK signaling, Arterioscler. Thromb. Vasc. Biol. 28 (2008) 127–134.
[48] C.H. Byon, A. Javed, Q. Dai, J.C. Kappes, T.L. Clemens, V.M. Darley-Usmar, J.M. McDonald, Y. Chen, Oxidative stress induces vascular calcification through modulation of the osteogenic transcription factor Runx2 by AKT signaling, J. Biol. Chem. 283 (2008) 15319–15327.
[49] I.M. Fenyo, I.C. Florea, M. Raicu, A. Manea Tyrphostin AG490 reduces NAPDH oxidase activity and expression in the aorta of hypercholesterolemic apolipoprotein E-deficient mice. *Vascul Pharmacol.* 201; 54:100-106.
[50] N.M. Gharavi, J.A. Alva, K.P. Mouillesseaux, C. Lai, M. Yeh, W. Yeung, J. Johnson, W.L. Szeto, L. Hong, M. Fishbein, L. Wei, L.M. Pfeffer, J.A. Berliner, Role of the Jak/STAT pathway in the regulation of interleukin-8 transcription by oxidized phospholipids in vitro and in atherosclerosis in vivo, J. Biol. Chem. 282 (2007) 31460–31468.
[51] J.F. Bentzon, C. Weile, C.S. Sondergaard, J. Hindkjaer, M. Kassem, E. Falk, Smooth muscle cells in atherosclerosis originate from the local vessel wall and not circulating progenitor cells in apoE knockout mice, Arterioscler. Thromb. Vasc. Biol. 26 (2006) 2696–2702.
[52] M.H. Hoofnagle, J.A. Thomas, B.R. Wamhoff, G.K. Owens, Origin of neointimal smooth muscle: we've come full circle, Arterioscler. Thromb. Vasc. Biol. 26 (2006) 2579–2581.
[53] S. Allahverdian, A.C. Chehroudi, B.M. McManus, T. Abraham, G.A. Francis, Contribution of intimal smooth muscle cells to cholesterol accumulation and macrophage-like cells in human atherosclerosis, Circulation 129 (2014) 1551–1559.
[54] M. Salmon, D. Gomez, E. Greene, L. Shankman, G.K. Owens, Cooperative binding of KLF4, pELK-1, and HDAC2 to a G/C repressor element in the SM22α promoter mediates transcriptional silencing during SMC phenotypic switching in vivo, Circ. Res. 111 (2012) 685–696.
[55] N. Sharma, Y. Lu, G. Zhou, X. Liao, P. Kapil, P. Anand, G.H. Mahabeleshwar, J.S. Stamler, M.K. Jain, Myeloid kruppel-like factor 4 deficiency augments atherogenesis in ApoE-/- mice–brief report, *Arterioscler Thromb. Vasc. Biol.* 32 (2012) 2836–2838.
[56] G. Zhou, A. Hamik, L. Nayak, H. Tian, H. Shi, Y. Lu, N. Sharma, X. Liao, A. Hale, L. Boerboom, R.E. Feaver, H. Gao, A. Desai, A. Schmaier, S.L. Gerson, Y. Wang, G.B. Atkins, B.R. Blackman, D.I. Simon, M.K. Jain, Endothelial kruppel-like factor 4 protects against atherothrombosis in mice, J. *Clin. Invest.* 122 (2012) 4727–4731.
[57] K.R. Cordes, N.T. Sheehy, M.P. White, E.C. Berry, S.U. Morton, A.N. Muth, T.H. Lee, J.M. Miano, K.N. Ivey, D. Srivastava, miR-145 and miR-143 regulate smooth muscle cell fate and plasticity, Nature 460 (2009) 705–710.
[58] P.M. Evans, W. Zhang, X. Chen, J. Yang, K.K. Bhakat, C. Liu, Kruppel-like factor 4 is acetylated by p300 and regulates gene transcription via modulation of histone acetylation, J. Biol. Chem. 282 (2007) 33994–34002.
[59] T. Boettger, N. Beetz, S. Kostin, J. Schneider, M. Kruger, L. Hein, T. Braun, Acquisition of the contractile phenotype by murine arterial smooth muscle cells depends on the miR143/145 gene cluster, J. Clin. Invest. 119 (2009) 2634–2647.
[60] F. Lovren, Y. Pan, A. Quan, K.K. Singh, P.C. Shukla, N. Gupta, B.M. Steer, A.J. Ingram, M. Gupta, M. Al-Omran, H. Teoh, P.A. Marsden, S. Verma, MicroRNA-145 targeted therapy reduces atherosclerosis, Circulation 126 (2012) S81–S90.
[61] Y. Vengrenyuk, H. Nishi, X. Long, M. Ouimet, N. Savji, F.O. Martinez, C.P. Cassella, K.J. Moore, S.A. Ramsey, J.M. Miano, E.A. Fisher, Cholesterol loading reprograms the microRNA-143/145-myocardin axis to convert aortic smooth muscle cells to a dysfunctional macrophage-like phenotype, Arterioscler. Thromb. Vasc. Biol. 35 (2015) 535–546.
[62] M. Chen, W. Li, N. Wang, Y. Zhu, X.R.O.S. Wang, and NF-kappaB but not LXR mediate IL-1beta signaling for the downregulation of ATP-binding cassette transporter A1, Am. J. Physiol. Cell Physiol. 292 (2007) C1493–C1501.
[63] N. Oyama, P. Gona, C.J. Salton, M.L. Chuang, R.R. Jhaveri, S.J. Blease, A.R. Manning, M. Lahiri, R.M. Botnar, D. Levy, M.G. Larson, C.J. O'Donnell, W.J. Manning, Differential impact of age, sex, and hypertension on aortic atherosclerosis: the Framingham Heart Study, Arterioscler. Thromb. Vasc. Biol. 28 (2008) 155–159.
[64] M. Pelat, C. Dessy, P. Massion, J.P. Desager, O. Feron, J.L. Balligand, Rosuvastatin decreases caveolin-1 and improves nitric oxide-dependent heart rate and blood pressure variability in apolipoprotein E-/- mice in vivo, Circulation 107 (2003) 2480–2486.
[65] D. Weiss, J.J. Kools, W.R. Taylor, Angiotensin II-induced hypertension accelerates the development of atherosclerosis in apoe-deficient mice, Circulation 103 (2001) 448–454.
[66] G. Gavazzi, B. Banfi, C. Deffert, L. Fiette, M. Schappi, F. Herrmann, K.H. Krause, Decreased blood pressure in NOX1-deficient mice, FEBS Lett. 580 (2006) 497–504.
[67] A. Dikalova, R. Clempus, B. Lassegue, G. Cheng, J. McCoy, S. Dikalov, A. San Martin, A. Lyle, D.S. Weber, D. Weiss, W.R. Taylor, H.H. Schmidt, G.K. Owens, J.D. Lambeth, K.K. Griendling, Nox1 overexpression potentiates angiotensin II-induced hypertension and vascular smooth muscle hypertrophy in transgenic mice, Circulation 112 (2005) 2668–2676.